Pharm Res (2015) 32:2559–2578
DOI 10.1007/s11095-015-1644-z

RESEARCH PAPER

A Novel Approach for Analyzing the Dissolution Mechanism of Solid Dispersions

Yuanhui Ji • Raphael Paus • Anke Prudic • Christian Lübbert • Gabriele Sadowski

Received: 5 September 2014 / Accepted: 29 January 2015 / Published online: 27 February 2015

ABSTRACT

Purpose To analyze the dissolution mechanism of solid dispersions of poorly water-soluble active pharmaceutical ingredients (APIs), to predict the dissolution profiles of the APIs and to find appropriate ways to improve their dissolution rate.

Methods The dissolution profiles of indomethacin and naproxen from solid dispersions in PVP K25 were measured *in vitro* using a rotating-disk system (USP II). A chemical-potential-gradient model combined with the thermodynamic model PC-SAFT was developed to investigate the dissolution mechanism of indomethacin and naproxen from their solid dispersions at different conditions and to predict the dissolution profiles of these APIs.

Results The results show that the dissolution of the investigated solid dispersions is controlled by dissolution of both, API and PVP K25 as they codissolve according to the initial API loading. Moreover, the dissolution of indomethacin and naproxen was improved by decreasing the API loading in polymer (leading to amorphous solid dispersions) and increasing stirring speed, temperature and pH of the dissolution medium. The dissolution of indomethacin and naproxen from their amorphous solid dispersions is mainly controlled by the surface reaction, which implies that indomethacin and naproxen dissolution can be effectively improved by formulation design and by improving their solvation performance.

Conclusions The chemical-potential-gradient model combined with PC-SAFT can be used to analyze the dissolution mechanism of solid dispersions and to describe and predict the dissolution profiles of API as function of stirring speed, temperature and pH value of the medium. This work helps to find appropriate ways to improve the dissolution rate of poorly-soluble APIs.

KEY WORDS amorphous solid dispersions · chemical-potential-gradient model · drug release mechanism · PC-SAFT · poorly water-soluble pharmaceutical

ABBREVIATIONS

a	Activity (−)
A	Surface area (m^2)
A_f	Fraction of the area of the interface for the transport of molecules from the solution (−)
c	Concentration mol/m^3
$\Delta c_{p,0API}^{SL}$	Difference in solid and liquid heat capacities of the API (J/(mol K))
Δh_{0API}^{SL}	Heat of fusion of pure API (kJ/mol)
J	Dissolution rate (mol/(m^2 s))
k_B	Boltzmann's constant $1.38065*10^{-23}$ (J/K)
k_d	Diffusion rate constant (mol/(m^2 s))
k_e	Equilibrium-exchange rate between the solid and liquid phase (mol/(m^2 s))
k_{ij}	Binary interaction parameter (−)
k_S	Surface reaction rate constant (mol/(m^2 s))
k_t	Total rate constant of dissolution (mol/(m^2 s))
m^{seg}	Segment number (−)
n_{exp}	Number of experimental data points (−)
T_{0API}^{SL}	Melting temperature of API (K)
V	Volume (m^3)
w	API loading (−)
w	Axial fluid speed (m/s)
x	Concentration or solubility in mole fraction (−)
a	Helmholtz energy (J)
A^-	Ionized form of monoprotic weak-acidic API
API	Active pharmaceutical ingredient
ARD	Average relative deviation

Electronic supplementary material The online version of this article (doi:10.1007/s11095-015-1644-z) contains supplementary material, which is available to authorized users.

Y. Ji (✉) • R. Paus • A. Prudic • C. Lübbert • G. Sadowski
TU Dortmund, Department of Biochemical and Chemical Engineering
Laboratory of Thermodynamics, Emil-Figge-Str. 70
44227 Dortmund, Germany
e-mail: Yuanhui.Ji@bci.tu-dortmund.de

Y. Ji
e-mail: yuanhuiji@aliyun.com

calc	Calculated results
exp	Experimental data
H_3O^+	Hydronium ion
HA	Monoprotic weak-acidic API
IND	Indomethacin
K_a	Acid dissociation equilibrium constant
LLE	Liquid-liquid equilibrium
M	Average molar mass (g/mol)
N	Total number of particles (−)
NAP	Naproxen
N^{assoc}	Number of association sites (−)
PVP	Polyvinylpyrrolidone
R	Universal ideal gas constant (J/K/mol)
SLE	Solid–liquid equilibrium
t	Time (s)
T	Temperature (Kelvin) or (°C)
Z	Compressibility factor (−)

GREEK SYMBOLS

α	Proportionality constant (−)
β_{API}	Degree of API crystallinity (−)
γ	Activity coefficient (−)
θ	Ratio of the dissolution rate of API to that of polymer
$\varepsilon_{hb}^{A_iB_i}/k_B$	Association-energy parameter (K)
φ	Fugacity coefficient (−)
$\varnothing$	Constant fraction of molecules that strike the solid surface (−)
ω	Stirring speed (round/s)
v	Kinematic viscosity of the solution (m^2/s)
δ	Thickness of diffusion layer (m)
u/k_B	Dispersion-energy parameter (K)
$\kappa_{hb}^{A_iB_i}$	Association-volume parameter (−)
μ	Chemical potential (J/mol)
v_c	Enhancement of equilibrium-exchange rate resulting from convection (mol/(m^2 s))
v_r	Collision frequency (mol/(m^2 s))
ρ	Density (mol/Å^3) or (mol/L)
σ	Segment diameter (Å)

SUBSCRIPTS

API	Active pharmaceutical ingredient
i j	Component indexes
polymer	Polymer
0	Pure substance

SUPERSCRIPTS

A_iB_i	Association sites A and B of molecule i
assoc	Association
B	Bulk phase
dipole	Dipole-dipole interactions
disp	Dispersion
elec	Ionic interactions
hc	Hard chain
I	Solid–liquid interface
L	Liquid phase
L1	Amorphous API-rich phase
L2	Water-rich phase
res	Residual
S	Solid phase
SD	Solid dispersion
seg	Segment
SL	Solid–liquid

INTRODUCTION

The low aqueous solubility of many crystalline active pharmaceutical ingredients (APIs) often leads to a slow dissolution in the aqueous gastro-intestinal fluids of the body, which often results in an insufficient oral bioavailability (1–3). A solid dispersion, where the amorphous API is integrated into a polymer excipient for stabilization, is a promising approach to improve the dissolution rate of poorly water-soluble APIs (2,4,5). The investigation of the dissolution profiles as well as of the dissolution mechanisms of solid dispersions is particularly important to characterize the performance of the solid dispersions and for the design of optimized formulations with controllable dissolution kinetics.

The dissolution profiles of poorly water-soluble APIs in amorphous solid dispersions have been widely investigated (2,6–8). Meanwhile, various models (*e.g.* the Noyes-Whitney equation (9,10), the Weibull model (11), the Higuchi model (12,13), the Hixson-Crowell model (14,15), the Korsmeyer-Peppas model (16), the Baker-Lonsdale model (17), *etc.*) have been used to characterize the dissolution mechanism of the APIs. Craig (18) reviewed the theories of carrier- and API-controlled dissolution and proposed a mathematical model to understand the release behavior of APIs from their dispersions. Siepmann *et al.* (19) proposed a model based on Fick's second law of diffusion to describe the transport of water and API considering the API diffusivities, matrix swelling and dissolution. More recently, Langham *et al.* (20) developed a mathematical model combining particle dissolution and growth processes to describe the dissolution profiles of felodipine from dissolving solid dispersion compacts. However, due to the high complexity of the solid-dispersion dissolution, it is very difficult to analyze the dissolution mechanism of APIs by theoretical models (15,18,20–22). Only few studies have been focused on the fundamental understanding of solid dispersion dissolution (20). The fundamental processes that govern the dissolution and the mechanisms of dissolution enhancement for solid dispersions are still not well understood (2,8,18). Therefore, it is necessary to systematically investigate the dissolution profiles of solid dispersions and to develop a theoretical model for describing their dissolution mechanism.

In this work, indomethacin (IND) and naproxen (NAP) were selected as model APIs and polyvinylpyrrolidone (PVP K25) with an average molar mass of 25,700 g/mol was selected as a model hydrophilic polymeric excipient. The chemical structures of the APIs and polymer are shown in Fig. 1.

Solid dispersions with different API loadings (w_{API}) in the polymer were prepared by spray drying. The dissolution profiles of the solid dispersions were measured by using a rotating-disk system (USP II).

Lu *et al.* (23) proposed a theoretical model and used it to describe the dissolution mechanism of inorganic salts (23–25). Based on that, a chemical-potential-gradient model was developed in this work to investigate the dissolution mechanism of solid dispersions. As the Perturbed-Chain Statistical Associating Fluid Theory (PC-SAFT) has been successfully applied to model solid–liquid equilibria of APIs (26,27) and amino acids (28,29) in solvents, phase behavior of polymer/solvent (30–32) and API/(co)polymer systems (33–35), and of systems including electrolytes (36–38), polar components (39,40) as well as to predict the "oiling-out" phenomenon (liquid-liquid equilibrium) in crystallization processes (41). Therefore, in this work, PC-SAFT (42) was applied to calculate the solubility and activity coefficient of API in solution. The effects of API loading, type of API, stirring speed, temperature, as well as of pH of the dissolution medium were investigated. Finally, the dissolution profiles of API at different conditions were calculated and even predicted.

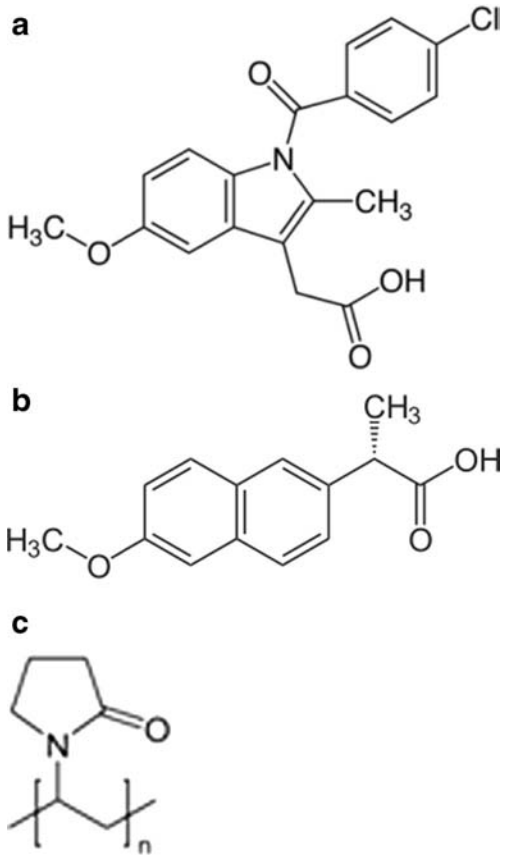

Fig. 1 Chemical structures of indomethacin (IND, **a**), naproxen (NAP, **b**) and polyvinylpyrrolidone (PVP K25, **c**).

THEORETICAL MODELING

Chemical-Potential-Gradient Model

The dissolution process of solid dispersions is depicted schematically in Fig. 2.

It includes two consecutive steps (23,43,44). In the first step, the release of API and polymer from the tablet and the hydration of the API and polymer molecules take place. This step is called "surface reaction" (23,43,44). Here, the difference of the API or polymer chemical potentials in the solid phase and the solid–liquid interface is the driving force of the surface reaction. The second step is the diffusion of the hydrated API and polymer molecules from the solid–liquid interface into the solution bulk phase (23,43,44). This time, the difference of the API or polymer chemical potential in the solid–liquid interface and the bulk phase is the driving force for the diffusion.

Surface-reaction rate and diffusion rate are described according to Eqs. (1) and (2), respectively.

$$\mathcal{J}_i = k_S\left(\frac{\mu_i^S}{RT} - \frac{\mu_i^I}{RT}\right) \tag{1}$$

$$\mathcal{J}_i = k_d\left(\frac{\mu_i^I}{RT} - \frac{\mu_i^B}{RT}\right) \tag{2}$$

where μ_i^S, μ_i^I and μ_i^B are the chemical potentials of the API or polymer in the solid phase, the solid–liquid interface and the

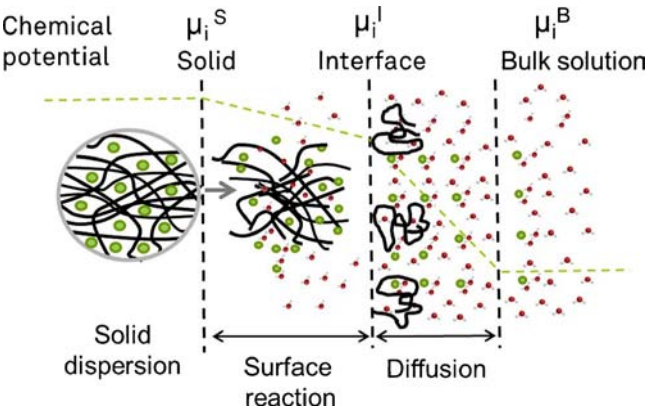

Fig. 2 Schematic picture of dissolution process of solid dispersions. μ_i^S, μ_i^I and μ_i^B represent the chemical potential of API or polymer in the solid phase, at the solid–liquid interface, and in the bulk phase, respectively.

bulk phase in J/mol, respectively. k_S and k_d are the rate constants of surface reaction and diffusion in mol/(m^2 s); R is the universal ideal gas constant in J/(mol K) and T is the temperature in Kelvin. By comparing the rate constants of surface reaction and diffusion, the rate-controlling step of the API or polymer dissolution can be determined. For k_S smaller than k_d, API or polymer dissolution is controlled by surface reaction. In the case that k_d is close to or equal to k_S, both surface reaction and diffusion are equally important and the API or polymer dissolution is controlled by both steps. If k_d is smaller than k_S, the dissolution is controlled by diffusion.

The chemical potential of the API or polymer at the solid–liquid interface μ_i^I and in the bulk phase μ_i^B are calculated by Eqs. (3) and (4), respectively.

$$\mu_i^I = \mu_{0i}^L + RT\ln a_i^I \tag{3}$$

$$\mu_i^B = \mu_{0i}^L + RT\ln a_i^B \tag{4}$$

where μ_{0i}^L is the chemical potential of API or polymer in the standard state (here pure component). a_i^I is the activity of API or polymer at the solid–liquid interface and is determined from the Statistical Rate Theory (45–47), which will be introduced in the following section. a_i^B is the activity of the API or polymer in the bulk phase and is calculated from the (time-dependent) mole fractions of API or polymer x_i^B in the bulk phase and the corresponding API or polymer activity coefficients γ_i^B, according to Eq. (5). The activity coefficient of the API or polymer can be calculated using a thermodynamic model (in this work PC-SAFT (42)).

$$a_i^B = x_i^B \gamma_i^B \tag{5}$$

Based on the phase-equilibrium principles, the chemical potential of the API or polymer in the solid phase μ_i^S equals that in its saturated solution according to Eq. (6).

$$\mu_i^S = \mu_i^L = \mu_{0i}^L + RT\ln a_i^L \tag{6}$$

where, μ_i^L and a_i^L are the chemical potential and activity of API or polymer in its saturated solution, respectively. For a crystalline API or polymer, the activity of the API or polymer in its saturated solution a_i^L is calculated based on the solid–liquid equilibrium, while for an amorphous solid API or polymer, the activity of the API or polymer a_i^L is calculated based on a liquid-liquid equilibrium (33). The theory of solid–liquid and liquid-liquid equilibrium as well as PC-SAFT will be introduced in following sections.

By substituting Eqs. (3), (4) and (6) into Eqs. (1) and (2), the following Eqs. (7) and (8) are obtained.

$$J_i = k_S \left(ln\, a_i^L - ln\, a_i^I\right) \tag{7}$$

$$J_i = k_d \left(ln\, a_i^I - \ln a_i^B\right) \tag{8}$$

By combining Eqs. (7) and (8) with the Statistical Rate Theory, the rate constants of surface reaction and diffusion can be determined and further the rate-controlling step of the solid dispersion dissolution can be analyzed.

Statistical Rate Theory

By using a first-order-perturbation analysis of the Schrödinger equation combined with the Boltzmann definition of entropy, Dejmek and Ward (45–47) developed the Statistical Rate Theory to describe the instantaneous molecular transport across a gas-liquid interface and a solid–liquid interface. This theory can be applied to describe the transport rate of APIs or polymer at the solid–liquid interface (shown in Fig. 2) according to Eq. (9).

$$J_i = k_e \left[\exp\left(\frac{\mu_i^S - \mu_i^I}{RT}\right) - \exp\left(\frac{\mu_i^I - \mu_i^S}{RT}\right)\right] \tag{9}$$

By substituting Eqs. (3) and (6) into Eq. (9), the following Eq. (10) is obtained.

$$J_i = k_e \left(\frac{a_i^L}{a_i^I} - \frac{a_i^I}{a_i^L}\right) \tag{10}$$

Equation (10) can be used to determine the activity of API or polymer at the solid–liquid interface a_i^I. In Eq. (10), k_e is the equilibrium-exchange rate between the solid and liquid phase per unit area of the interface, which is calculated according to Eq. (11).

$$k_e = v_r \cdot A_f + v_c \cdot A_f \tag{11}$$

where A_f is the fraction of the area of the interface for the transport of molecules from the solution and it is considered as a constant. v_r is the collision frequency of the solute molecules with the solid surface that results from their random motion at equilibrium conditions in mol/(m^2 s), and v_c is the enhancement of this rate that results from convection in mol/

(m^2 s). The collision frequency v_r is proportional to $x_i^L\sqrt{T}$ as described by Eq. (12).

$$v_r = \alpha_1 x_i^L \sqrt{T} \tag{12}$$

Here, x_i^L is the solubility of API or polymer in mole fraction, α_1 is a proportionality constant and T is the temperature in Kelvin.

v_c is expressed as

$$v_c = -\alpha_2 x_i^L \varnothing w(\delta) \tag{13}$$

where α_2 is a proportionality constant in mol/m^3, $\varnothing$ a constant fraction of molecules that strike the solid surface, and $w(\delta)$ is the axial fluid speed in m/s, which is calculated according to Eq. (14).

$$w(\delta) = -0.510\sqrt{\frac{\omega^3}{v}}\delta^2 \tag{14}$$

Here, v is the kinematic viscosity of the solution in m^2/s, δ the thickness of diffusion layer in m, and ω the stirring speed in round/s. Combining Eqs. (11)–(14), the equilibrium exchange rate k_e between the solid and liquid phase per unit area of the interface can be expressed by Eq. (15).

$$k_e = \alpha_1 A_f x_i^L \sqrt{T} + 0.510\alpha_2 \varnothing A_f x_i^L \sqrt{\frac{\omega^3}{v}}\delta^2 \tag{15}$$

It is set that $K_1 = \alpha_1 A_f$ and $K_2 = \alpha_2 \varnothing A_f \delta^2$. The parameters k_d, k_s, K_1, and K_2 were fitted to the experimental dissolution profiles using Eqs. (7), (8), and (10).

Modeling and Prediction of Dissolution Profiles

In Eqs. (7), (8) and (10), $\mathcal{J}_i$ represents the rates of the surface reaction and diffusion and of API or polymer transport rate at the solid–liquid interface in mol/(m^2 s) and is calculated according to Eq. (16).

$$\mathcal{J}_i = \frac{1}{A} \cdot V \cdot \frac{dc_i^B}{dt} \tag{16}$$

In Eq. (16), A is the surface area in m^2 of the dissolving API or polymer contacting the dissolution medium. In this work, the surface area is calculated as the base area of a cylindrical tablet and it is considered as a constant. V is the volume of the dissolution medium in m^3 and c_i^B is the (time-dependent) concentration of the API or polymer in the bulk phase in mol/m^3. t is the time in s.

The dissolution rates of API and polymer may have the following relation:

$$\mathcal{J}_{API} = \mathcal{J}_{polymer} \cdot \theta(w_{API}) \tag{17}$$

In Eq. (17), $\mathcal{J}_{API}$ and $\mathcal{J}_{polymer}$ are the dissolution rates of API and polymer, respectively. $\theta(w_{API})$ represents the ratio of the dissolution rate of API to that of polymer and is considered as being a function of API loading (w_{API}) in the solid dispersion.

According to Eqs. (1) and (2), the dissolution rate of the API or polymer can be expressed by the total rate constant of API or polymer dissolution k_t and the difference of the API or polymer chemical potential in the solid phase and the bulk phase $\left(\frac{\mu_i^S}{RT} - \frac{\mu_i^B}{RT}\right)$, as shown in Eq. (18).

$$\mathcal{J}_i = k_t\left(\frac{\mu_i^S}{RT} - \frac{\mu_i^B}{RT}\right) = k_t\left(ln\, a_i^L - ln\, a_i^B\right) \tag{18}$$

k_t is the total rate constant of API or polymer dissolution and is calculated from the rate constants of surface reaction k_s and diffusion k_d as shown in Eq. (19).

$$k_t = \frac{1}{\frac{1}{k_d} + \frac{1}{k_s}} \tag{19}$$

By combining Eqs. (16), (18) and (19) with a thermodynamic model for calculating the activity coefficients of the API or polymer, the dissolution profiles of the API or polymer at various conditions can be calculated and even predicted. If the quantitative relation of the dissolution rate of API and that of polymer ($\theta(w_{API})$ in Eq. (17)) is obtained, the dissolution profiles of API can also be predicted based on the dissolution profiles of the polymer according to Eq. (17).

Solid–liquid Equilibrium

For a crystalline API, its chemical potential in the solid phase equals that in its saturated solution according to the solid–liquid equilibrium (SLE), as shown in Eq. (20).

$$\mu_{API}^S = \mu_{API}^L \tag{20}$$

where, μ_{API}^S is the chemical potential of the crystalline API in the solid phase, μ_{API}^L is the chemical potential of the API in its

saturated solution, and it can be calculated according to Eq. (6).

Assuming that the crystalline API in the solid phase is a pure component (26,48), its solubility x_{API}^{L} in mole fraction can be calculated according to Eq. (21).

$$x_{API}^{L} = \frac{1}{\gamma_{API}^{L}} \exp\left\{ -\frac{\Delta h_{0API}^{SL}}{RT}\left(1-\frac{T}{T_{0API}^{SL}}\right) - \frac{\Delta c_{p,0API}^{SL}}{R}\left[\ln\left(\frac{T_{0API}^{SL}}{T}\right) - \frac{T_{0API}^{SL}}{T} + 1\right]\right\} \tag{21}$$

where Δh_{0API}^{SL}, T_{0API}^{SL}, and $\Delta c_{p,0API}^{SL}$ are the heat of fusion, the melting temperature, and the difference in solid and liquid heat capacities of the crystalline API, respectively. These properties can be determined experimentally (*e.g.* by differential scanning calorimetry measurements). γ_{API}^{L} is the activity coefficient of the API in its saturated solution, which is used to identify the non-ideality of the system and often depends on temperature and on the concentration of the API in solution. In this work, PC-SAFT (42) was applied to calculate the activity coefficients and therewith the solubility of the API in aqueous media.

Liquid-Liquid Equilibrium

For an amorphous API, its chemical potential and the chemical potential of water in an amorphous API-rich phase L1 equals those in a water-rich phase L2 according to the liquid-liquid equilibrium (LLE) (33), as shown in Eqs. (22) and (23).

$$\mu_{API}^{L1} = \mu_{API}^{L2} \tag{22}$$

$$\mu_{water}^{L1} = \mu_{water}^{L2} \tag{23}$$

where, μ_{API}^{L1} and μ_{water}^{L1} are the chemical potentials of the amorphous API and water in an API-rich phase L1, μ_{API}^{L2} and μ_{water}^{L2} are the chemical potentials of the API and water in a water-rich phase L2. Based on Eqs. (22) and (23), the following equations are derived.

$$x_{API}^{L1} \cdot \gamma_{API}^{L1} = x_{API}^{L2} \cdot \gamma_{API}^{L2} \tag{24}$$

$$x_{water}^{L1} \cdot \gamma_{water}^{L1} = x_{water}^{L2} \cdot \gamma_{water}^{L2} \tag{25}$$

where x_{API}^{L1}, x_{API}^{L2}, x_{water}^{L1} and x_{water}^{L2} are the mole fractions of the API and water in both liquid phases L1 and L2. Here, x_{API}^{L2} is the solubility of the amorphous API in water. γ_{API}^{L1} and γ_{API}^{L2} are the activity coefficients of API in the two phases; and γ_{water}^{L1} and γ_{water}^{L2} are the activity coefficients of water in the two phases. Here, PC-SAFT (42) was also applied to calculate the activity coefficients of the API and water in both phases.

Calculation of pH-dependent API Solubility

A monoprotic weak-acidic API (HA) dissociates into its ionized form A^- and a proton which forms a hydronium ion (H_3O^+) in an aqueous solution as shown in Eq. (26).

$$HA + H_2O \rightleftharpoons H_3O^+ + A^- \tag{26}$$

The concentrations (in mol/L) of the charged [A^-] and non-charged API species [HA] are determined based on its acid dissociation equilibrium constant K_a according to Eq. (27).

$$K_a = \frac{[H_3O^+][A^-]}{[HA]} \tag{27}$$

Here, the concentration of the non-charged API species [HA] is called the API intrinsic solubility. The API solubility is the total concentration of the dissolved API species $[HA]_T$, which is calculated according to Eq. (28).

$$[HA]_T = [HA] + [A^-] \tag{28}$$

According to the identical concentrations of the hydronium ions and the charged API species [A^-], the API intrinsic solubility [HA] can be calculated based on its solubility in water and K_a value by combining Eqs. (27) and (28). The pK_a value of indomethacin was taken as being 4.5 from literature (49). The solubility of amorphous indomethacin at a certain pH is calculated by using the Henderson-Hasselbalch equation (50–53) as shown in Eq. (29).

$$[HA]_T(pH) = [HA]\left(1 + 10^{pH-pK_a}\right) \tag{29}$$

PC-SAFT

Within PC-SAFT, the residual Helmholtz energy a^{res} of a system is calculated as the sum of different contributions (42,54). Depending on the nature of the investigated molecules, the Helmholtz-energy contributions could be attributed to repulsion (hard-chain contribution a^{hc}), van der Waals attraction (dispersive contribution a^{disp})

(42), association (hydrogen bonding, a^{assoc}) (54), ionic interactions (a^{elec}) (36–38) and dipole-dipole interactions (a^{dipole}) (39), as shown in Eq. (30):

$$a^{res} = a^{hc} + a^{disp} + a^{assoc} + a^{elec} + a^{dipole} \tag{30}$$

The detailed expressions of these contributions within PC-SAFT are described elsewhere in earlier publications (36–39,42,54), and are not shown in detail here.

PC-SAFT considers a molecule as a chain which consists of m^{seg} spherical segments with a diameter σ. A non-associating component can be modeled using the following three pure-component parameters: the segment number (m^{seg}), the segment diameter (σ), and the dispersion-energy parameter (u/k_B). To characterize an associating component (molecules which are able to interact with each other by hydrogen bonding, as indomethacin and naproxen) and polymers (PVP K25), two additional parameters are required: the association-energy parameter ($\varepsilon_{hb}^{A_iB_i}/k_B$, k_B is the Boltzmann's constant), and the association-volume parameter ($\kappa_{hb}^{A_iB_i}$). Furthermore, the number of the association sites (N^{assoc}) which can act as proton donators and acceptors is required for each molecule and is usually determined based on the molecular structure of the component.

To describe the Helmholtz energy of mixtures, the Berthelot-Lorentz combining rules are applied to represent the interactions between different components i and j, as shown in Eqs. (31) and (32).

$$\sigma_{ij} = \frac{1}{2}\left(\sigma_i + \sigma_j\right) \tag{31}$$

$$u_{ij} = \left(1-k_{ij}\right)\sqrt{u_i u_j} \tag{32}$$

As shown in Eq. (32), one adjustable binary interaction parameter (k_{ij}) is introduced to correct for the dispersion-energy parameter for the mixture of components i and j. Sometimes k_{ij} is dependent on temperature as described in Eq. (33).

$$k_{ij} = k_{ij,T}\cdot T + k_{ij,0} \tag{33}$$

with $k_{ij,T}$ and $k_{ij,0}$ being parameters which are fitted to binary data.

To describe the cross-association interactions between two different associating components, simple mixing and combining rules suggested by Wolbach and Sandler (55) are applied according to Eqs. (34) and (35). Here, no additional adjustable binary parameters are required.

$$\varepsilon_{hb}^{A_iB_j} = \frac{1}{2}\left(\varepsilon_{hb}^{A_iB_i} + \varepsilon_{hb}^{A_jB_j}\right) \tag{34}$$

$$\kappa_{hb}^{A_iB_j} = \sqrt{\kappa_{hb}^{A_iB_i}\,\kappa_{hb}^{A_jB_j}}\left[\frac{\sqrt{\sigma_{ii}\sigma_{jj}}}{(1/2)\left(\sigma_{ii}+\sigma_{jj}\right)}\right]^3 \tag{35}$$

Calculation of Activity Coefficient from PC-SAFT

From the residual Helmholtz energy of a system (a^{res}), the residual chemical potential (μ_i^{res}) of the API or polymer can be calculated (26) according to Eq. (36).

$$\frac{\mu_i^{res}}{k_BT} = \frac{a^{res}}{k_BT} + Z - 1 + \left[\frac{\partial\left(a^{res}/k_BT\right)}{\partial x_i}\right] - \sum_{j=1}^{N}\left[x_j\left(\frac{\partial\left(a^{res}/k_BT\right)}{\partial x_j}\right)\right] \tag{36}$$

where Z is the compressibility factor, which is calculated in terms of the residual Helmholtz energy (a^{res}) (26) according to Eq. (37).

$$Z = 1 + \rho\left[\frac{\partial\left(a^{res}/k_BT\right)}{\partial\rho}\right] \tag{37}$$

where ρ is the density of the system.

The fugacity coefficient of the API or polymer in a mixture is calculated based on its residual chemical potential (μ_i^{res}) (26) according to Eq. (38).

$$\ln\varphi_i^L = \frac{\mu_i^{res}}{k_BT} - \ln Z \tag{38}$$

The activity coefficient of the API or polymer is defined as a ratio of its fugacity coefficient in the mixture (φ_i^L) to that of the pure component φ_{0i}^L:

$$\gamma_i^L = \frac{\varphi_i^L}{\varphi_{0i}^L} \tag{39}$$

MATERIALS AND METHODS

Materials

Crystalline indomethacin in γ-form with a purity of more than 99% was purchased from Sigma-Aldrich Co. LLC (Hamburg, Germany). Crystalline naproxen with a purity of more than 99% was purchased from TCI Deutschland GmbH (Eschborn, Germany). The polymer PVP K25 (Kollidon® K25) was purchased from BASF (Ludwigshafen, Germany). Ethanol and acetone with a purity of more than 95% were used as solvents to dissolve the APIs and the polymer for spray drying and were supplied by VWR International S.A.S. (Fontenay-sous-Bois, France) and by Merck KGaA (Darmstadt, Germany). Di-sodium hydrogen phosphate dihydrate and potassium dihydrogen phosphate were purchased from Merck KGaA (Darmstadt, Germany) and used for preparation of dissolution media with different pH values. Water from a Millipore purification system was used for the preparation of all aqueous solutions for the dissolution measurements.

Methods

Spray Drying

Solid dispersions of indomethacin and naproxen in PVP K25 with different API loadings (weight fractions) of 0.2, 0.4, 0.6 and 0.8 were prepared *via* a Büchi mini spray dryer B-290 (Büchi Company, Switzerland). The powders were produced by spray drying from solutions in which API and PVP K25 were dissolved in ethanol for indomethacin and in acetone for naproxen at a concentration of 15 g/L. The inlet temperature of the spray dryer was set to 120°C for indomethacin and to 85°C for naproxen. The aspirator was set to 100%, the feed rate of the solution was 7 ml/min, and the flow rate of nitrogen was 550 l/h. All spray-dried powders were dried in a climate chamber at room temperature and vacuum condition for at least 24 h to remove the remaining water and organic solvent prior to physicochemical characterization and dissolution measurements. All powders were further stored in the climate chamber at room temperature and vacuum condition.

Analysis of Homogeneity

The homogeneity of indomethacin and naproxen solid dispersions was investigated following the procedures in the standard method (ISO 13528:2005) (56). Ten samples of the solid dispersions (0.5–2.5 g each) were selected randomly from each prepared and dried product. They were weighted with an accuracy of ±0.3 mg, dissolved in a 50/50 (*v*/*v*) ethanol/water solution and the API concentrations were determined using an UV–Vis spectrophotometer (Jena, Germany). Each measurement was performed in triplicates. The API compositions in the ten different samples were determined and were used to evaluate the homogeneity according to the standard method (ISO 13528:2005) (56).

Modulated Temperature Differential Scanning Calorimetry (mDSC)

The solid state of solid dispersions was characterized by the DSC measurements using a Q 2000 modulated DSC (TA Instruments, Eschborn, Germany). The apparatus was calibrated using indium. Nitrogen was purged into the DSC cell at a flow rate of 50 mL/min to maintain the inert atmosphere. The solid dispersion samples of 10 to 20 mg were added into aluminum pans and weighted with an accuracy of ±0.3 mg and then heated from 283.15 to 443.15 K at a heating rate of 2 K/min. The samples were equilibrated at 283.15 K for 5 min before heating. The modulation amplitude was set at ±0.318 K, and the modulation period was set to 60 s. Each measurement was performed at least twice. The measured results were analyzed mathematically using the TA Universal Analysis 2000 (TA Instruments, Eschborn, Germany). If melting took place during heating, the melting peaks were analyzed to determine the degree of API crystallinity. The degree of API crystallinity, β_{API} (%) in solid dispersions was estimated from the melting enthalpies of pure API and the API in the solid dispersion using the following Eq. (40).

$$\beta_{API}\ (\%) = \frac{\Delta h^{SL}_{SD,\ API}}{\Delta h^{SL}_{0API} \times w_{API}} \times 100 \tag{40}$$

where Δh^{SL}_{0API} and $\Delta h^{SL}_{SD,\ API}$ are the melting enthalpies of pure API and the API in the solid dispersion, respectively. These properties (Δh^{SL}_{0API} and $\Delta h^{SL}_{SD,\ API}$) were determined experimentally by mDSC in this work.

Powder X-ray Diffraction (PXRD)

The solid state of the solid dispersions was also characterized by PXRD. The measurements were performed at room temperature using a Philips X-ray Powder Diffractometer (Germany) with Cu-K alpha irradiation (λ = 1.544), voltage of 35 kV and current of 30 mA. The data were collected in step scan mode in the region of $10° \leq 2\theta \leq 40°$ with a step size of 0.05°.

Scanning Electron Microscopy (SEM)

The particle sizes and morphologies of the raw materials and different solid dispersions of indomethacin and naproxen were observed using the SEM (HITACHI S-4500, Japan) at the working distance of 9 mm and an accelerated voltage of 1 kV.

Preparation of Dissolution Media

A $Na_2HPO_4{\cdot}2H_2O/KH_2PO_4$ buffer was used to prepare dissolution media at different pH values of 5.0, 6.0 and 7.2 (53). The exact pH values of the media were measured with a pH meter (Mettler-Toledo GmbH, Gießen, Germany). In order to reduce the air bubbles in the media, the media were degassed by purging helium for one and a half hours prior to the dissolution measurement.

In-vitro Intrinsic Dissolution Measurement

The dissolution profiles of indomethacin and naproxen solid dispersions in water and in buffered solutions were measured using a rotating disk system (USP II). This apparatus includes a dissolution measurement device (SOTAX AT 7 smart, SOTAX GmbH, Allschwil, Switzerland) and an UV–Vis spectrophotometer (Jena, Germany). Tablets of solid dispersions with a diameter of 8 mm were prepared by pressing the weighted powders in the disk die with a force of 2 kN. After that, they were inserted into the dissolution vessel which contained 500 mL of dissolution medium. To investigate the influence of API loading on solid-dispersion dissolution at a temperature of 310.15 K (accuracy ± 0.3 K) and a stirring speed of 50 rpm, 200 mg samples were used for each tablet, while for investigating the influence of temperature, stirring speed and pH on solid-dispersion dissolution at a fixed API loading of 0.8, 80 mg samples were used for each tablet.

UV–Vis Spectrophotometric Analysis

The absorbance of the samples was measured using an UV–Vis spectrophotometer (Jena, Germany) at two different wavelengths (320 and 218 nm for indomethacin/PVP K25 solid dispersions, and 331 and 218 nm for naproxen/PVP K25 solid dispersions). The absorbance-wavelength curves of the aqueous solutions of indomethacin, naproxen and PVP K25 are shown in Figures S1 and S2 in the Supplementary Information. The wavelength of 218 nm was used since at this wavelength PVP K25 has almost the highest absorbance and the API (indomethacin or naproxen) has comparable absorbances to that of PVP K25. The samples were collected and measured every 15 min. Standard solutions of the APIs and PVP K25 at different concentrations were prepared and measured at the above-mentioned wavelengths for the APIs and at 218 nm for PVP K25 solutions to generate the calibration curves. The simultaneous release profiles of API and PVP K25 from the solid dispersions were analyzed using the quantitative multi-component-analysis method. In this method, the concentrations of indomethacin or naproxen were determined from their measured time-dependent absorbances at 320 and 331 nm of the samples during the dissolution of their respective solid dispersions. The absorbances of indomethacin or naproxen for each sample at 218 nm were then calculated based on their respective concentrations. After that, the absorbances of PVP K25 at 218 nm for each sample were calculated based on the measured total absorbances.

RESULTS

Analysis of Homogeneity

Figure 3 shows the homogeneity of the indomethacin and naproxen solid dispersions at various API loadings. It shows that the homogeneity of the solid dispersions is always higher than 94% and for most of the solid dispersions higher than 98%. It is also observed that the homogeneity of naproxen solid dispersions is higher than that of indomethacin solid dispersions. It can be concluded, that indomethacin and naproxen are homogeneously dispersed in the PVP K25 carrier for the solid dispersions prepared by spray drying in this work.

Measurement of degree of API Crystallinity *via* DSC

Figure 4a shows the DSC thermograms of indomethacin solid dispersions in PVP K25 at various indomethacin loadings. No melting peak is observed for indomethacin loadings of 0.2, 0.4 and 0.6. This reveals that these solid dispersions were amorphous. For solid dispersions with an indomethacin loading of 0.8, there are two small endothermal melting peaks shown in Fig. 4a. The first peak indicates the melting of crystalline α -indomethacin and the second one indicates that of γ -indomethacin. There is no obvious recrystallization peak shown here. Based on Eq. (40), and the melting enthalpies of pure α -indomethacin $\Delta h^{SL}_{0,\,IND\,\alpha}$ (32.92 kJ/mol from Ref. (57)) and γ

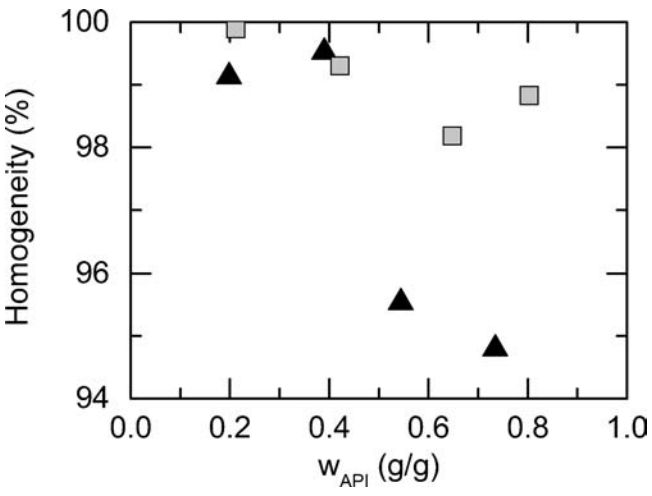

Fig. 3 Homogeneity of indomethacin and naproxen solid dispersions in PVP K25 at various API loadings. *Back triangles* represent the homogeneity of indomethacin solid dispersions and *gray squares* represent that of naproxen solid dispersions.

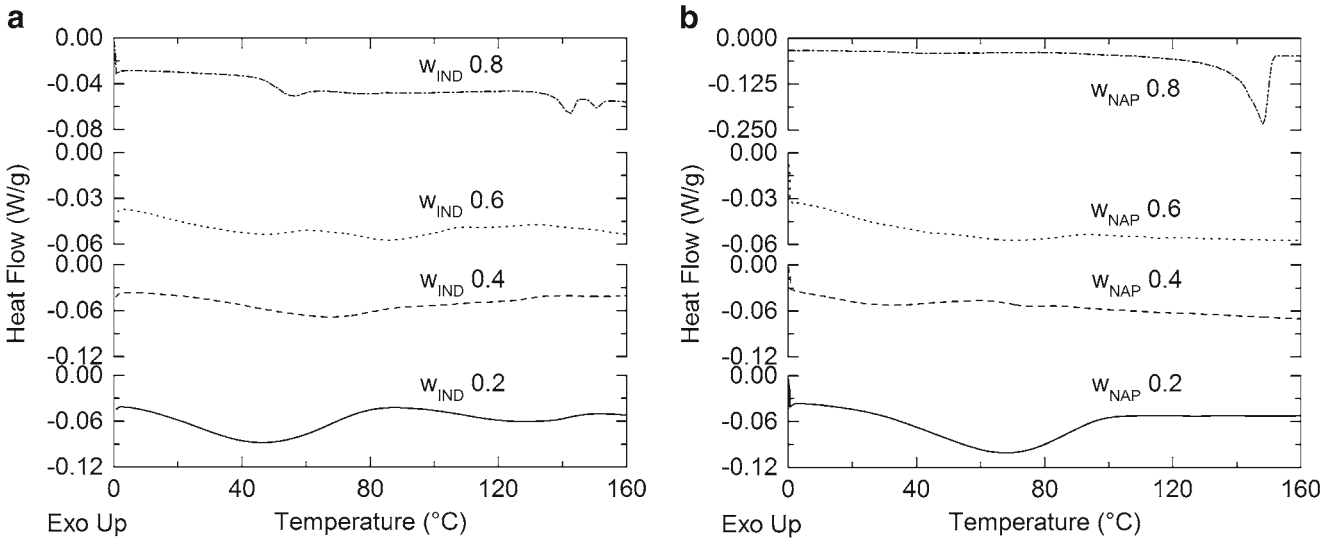

Fig. 4 DSC thermograms of indomethacin (**a**) and naproxen (**b**) solid dispersions in PVP K25 with various API loadings. The *full lines*, *dashed lines*, *dotted lines* and *dashed dotted lines* represent the thermograms of solid dispersions with API loadings of 0.2, 0.4, 0.6 and 0.8, respectively.

-indomethacin $\Delta h^{SL}_{0,\,IND\,\gamma}$ (39.2 kJ/mol from Ref. (53)) and that of indomethacin in solid dispersions $\Delta h^{SL}_{SD,\,IND}$ (determined from Fig. 4a), the degree of crystallinity of indomethacin solid dispersions with indomethacin loading of 0.8 is calculated as 3.59%, which indicates that 96.41% of the solid dispersion is amorphous.

Figure 4b shows the thermograms of naproxen solid dispersions at various naproxen loadings. No melting peak is observed for the solid dispersions with naproxen loadings of 0.2, 0.4 and 0.6, which reveals that these solid dispersions are amorphous. For solid dispersions with naproxen loading of 0.8, there is no obvious recrystallization peak, but one sharp endothermal melting peak as shown in Fig. 4b, which indicates the melting of crystalline naproxen. Based on Eq. (40) and the melting enthalpies of pure crystalline naproxen $\Delta h^{SL}_{0,NAP}$ and that of naproxen in solid dispersions $\Delta h^{SL}_{SD,\,NAP}$ (determined from Fig. 4b), the degree of crystallinity of naproxen solid dispersions with naproxen loading of 0.8 is calculated as an average of three measurements to a value of 49.55%, which indicates that almost half of the naproxen in the solid dispersions are crystalline.

Solid State of Solid Dispersion *via* PXRD

The solid state of indomethacin and naproxen solid dispersions with API loadings of 0.2, 0.4, 0.6 and 0.8 were further characterized by PXRD, and their diffraction patterns are shown in Fig. 5.

The X-ray diffraction patterns show amorphous hills without diffraction peaks for all indomethacin solid dispersions in PVP K25 (Fig. 5a) which indicates the amorphous state of these solid dispersions. As shown in Fig. 5b, naproxen solid dispersions with naproxen loadings of 0.2, 0.4 and 0.6 are also amorphous, while for naproxen solid dispersions with a naproxen loading of 0.8, the peaks at 2θ of 12.6°, 16.7°, 18.95°, 20.3°, 22.3°, 23.6°, 27.4° are observed. Those peaks are characteristics of crystalline naproxen, which reveals that naproxen solid dispersions with naproxen loading of 0.8 were crystalline. This observation agrees with the characterization results by DSC.

Morphology of Solid Dispersion *via* SEM

The particle sizes and morphologies of the raw materials of indomethacin and naproxen and their solid dispersions were characterized by the SEM. The images are shown in Fig. 6.

Figure 6a exhibits faceted morphologies of indomethacin, which shows the crystalline state of the raw material of indomethacin. Figure 6b–e show spherical morphologies of indomethacin solid dispersions with different indomethacin loadings, which implies the amorphous state of the solid dispersions. As shown in the small black boxes in Fig. 6e, there is small amount of rods lying in the powders, which indicates a low fraction (less than 5%) of crystalline indomethacin in the solid dispersions with indomethacin loading of 0.8. This observation is in good accordance with the crystallinity analysis (calculated as 3.59%) by DSC. Figure 6b–e also show that the particle size of all indomethacin solid dispersions is in a similar range and is much smaller than that of pure crystalline indomethacin (see Fig. 6a).

Figure 6f, j exhibits faceted morphologies of naproxen, which shows crystals of naproxen in raw materials and in the solid dispersion with a naproxen loading of 0.8. Figure 6g, h shows spherical morphologies and similar particle size range for naproxen solid dispersions with naproxen loadings of 0.2 and 0.4, which implies the amorphous state of the particles. It

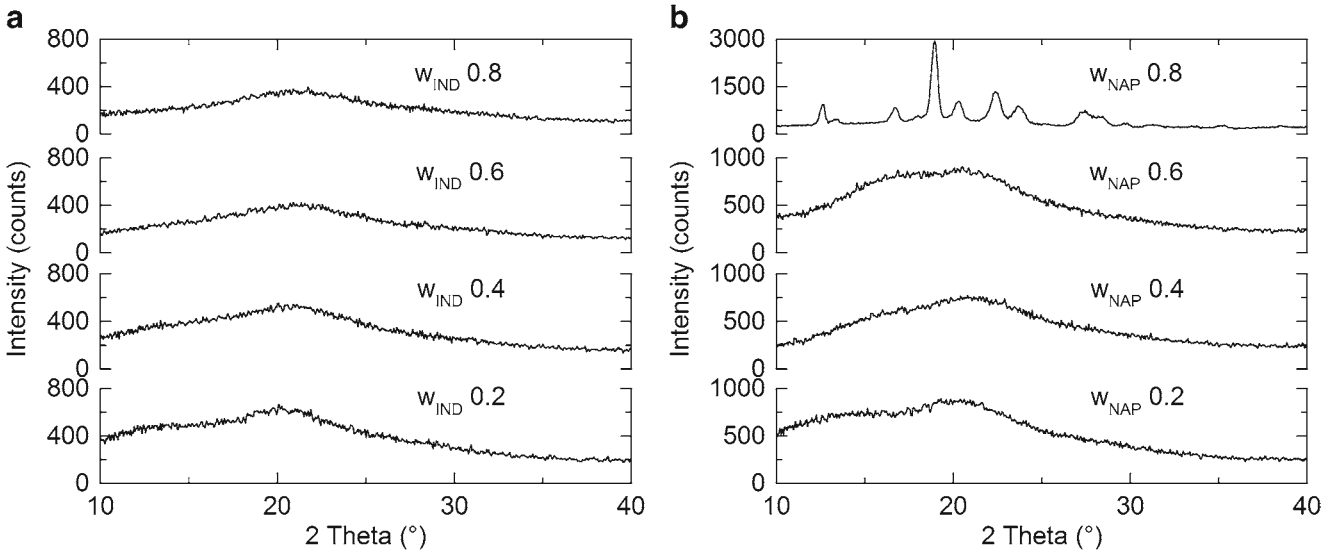

Fig. 5 X-ray diffraction spectra of indomethacin (**a**) and naproxen (**b**) solid dispersions with API loadings of 0.2, 0.4, 0.6 and 0.8.

is obvious that the particle size of naproxen solid dispersions with naproxen loadings of 0.2 and 0.4 is smaller than that of pure crystalline naproxen. Figure 6i shows compact forms of naproxen solid dispersions with naproxen loading of 0.6. Here, no faceted structure or rods which indicate naproxen crystals can be found on this image.

DISCUSSION

PC-SAFT Parameters

The pure-component parameters of indomethacin, naproxen, PVP K25, water and buffer components (K^+, Na^+, $H_2PO_4^-$,

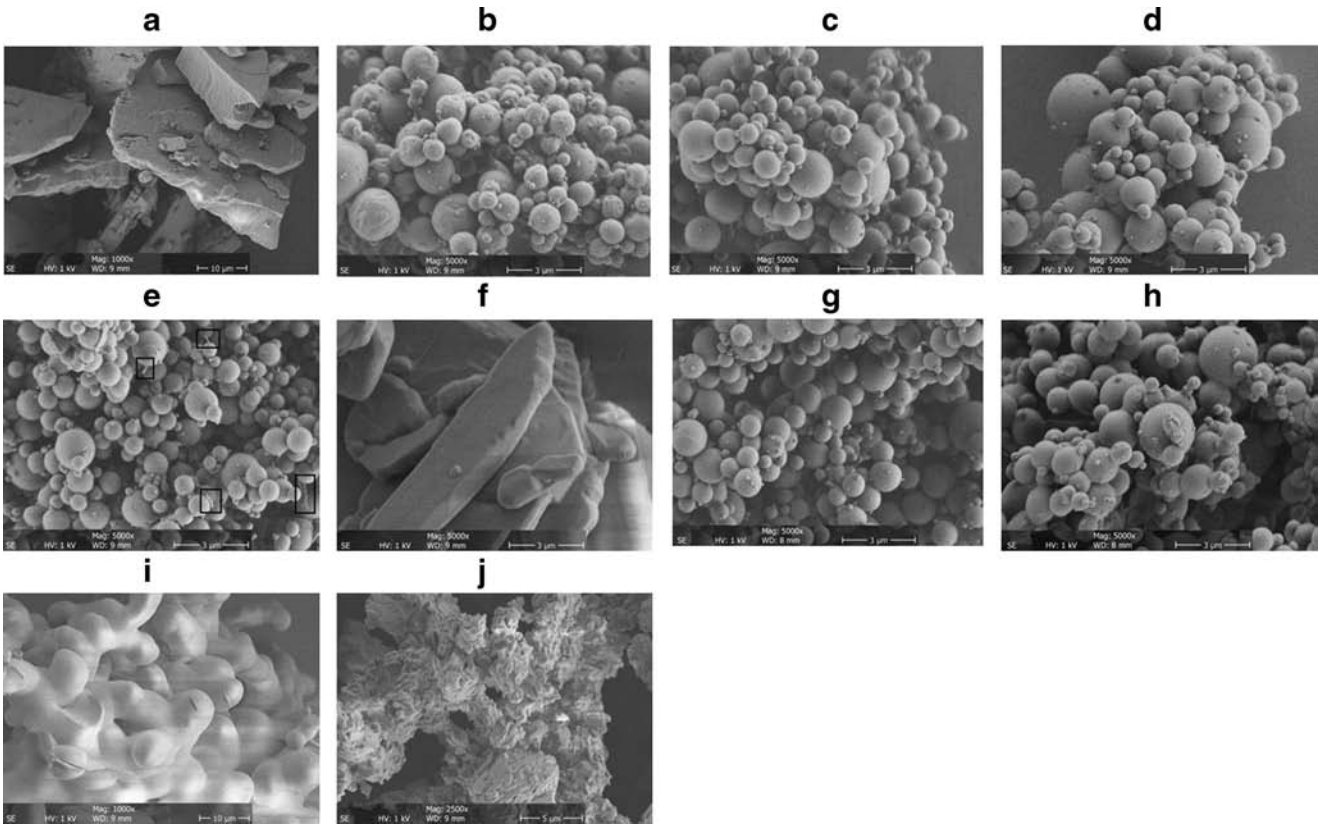

Fig. 6 SEM images of raw materials of indomethacin (**a**) and naproxen (**f**) and their solid dispersions in PVP K25. **b**–**e**: indomethacin solid dispersions with indomethacin loadings of 0.2 (**b**), 0.4 (**c**), 0.6 (**d**) and 0.8 (**e**). **g**–**j**: naproxen solid dispersions with naproxen loadings of 0.2 (**g**), 0.4 (**h**), 0.6 (**i**), 0.8 (**j**).

Table I Molecular Weights and Pure-Component PC-SAFT Parameters of Indomethacin, Naproxen, PVP K25, Water and Buffer Components Used in this Work

Component	M (g/mol)	m^{seg} (−)	σ (Å)	u/k_B (K)	$\varepsilon_{hb}^{A_iB_i}/k_B$ (K)	$\kappa_{hb}^{A_iB_i}$ (−)	N^{assoc} (−)	Ref.
Indomethacin	357.79	14.283	3.535	262.79	886.4	0.02	3/3	(33)
Naproxen	230.26	8.111	2.938	229.45	934.2	0.02	2/2	(34)
PVP K25	25700	1045.2	2.710	205.59	0	0.0451	231/231	
Water	18.02	1.205	σ_{water} [a]	353.95	2425.7	0.0451	1/1	(28)
K^+	39.10	1	3.342	200	–	–	–	(58)
Na^+	22.99	1	2.823	230	–	–	–	(58)
$H_2PO_4^-$	96.99	1	3.651	95	–	–	–	(58)
HPO_4^{2-}	95.98	1	2.162	146.02	–	–	–	(58)

[a] $\sigma_{water} = 2.7927 + 10.11 \cdot \exp(-0.01775 \cdot T) - 1.417 \cdot \exp(-0.01146 \cdot T)$ (28)

HPO_4^{2-}) and the binary interaction parameters between API and PVP K25, between API and water, between PVP K25 and water as well as those between the buffer components and water were taken from literature (28,33,34,53,58). These parameters as well as the melting properties of the APIs used for the modeling are listed in Tables I, II, and III. It needs to be noted that PVP K25 was treated as a molecule with induced association and the association-volume parameter of PVP K25 was set equal to the one of water.

API Solubility in Water and in Buffered Solutions

Using the parameters from Tables I, II, and III, the solubility of crystalline naproxen in water was calculated from SLE (see Eq. (21)) and those of amorphous naproxen and indomethacin in water were calculated from LLE (see Eqs. (24) and (25)) with PC-SAFT as described in Sections "Solid-liquid Equilibrium", "Liquid-liquid Equilibrium" and "PC-SAFT".

The solubility of amorphous indomethacin at a certain pH is calculated by using Eq. (29). The calculated solubilities are listed in Tables IV and V.

As shown in Table IV, the calculated solubilities of both, crystalline and amorphous naproxen and those of amorphous indomethacin increase with increasing temperature. Moreover, the solubility of amorphous naproxen is more than ten times higher than that of its crystalline form, and the solubility of amorphous naproxen is more than five times higher than that of amorphous indomethacin.

As shown in Table V, as indomethacin is a weak acid, the calculated solubility of amorphous indomethacin increases with increasing pH.

These calculated solubility data were further used for modeling the dissolution of API from solid dispersions.

In order to determine the API activity coefficient in the buffer system, the compositions of buffer components (K^+, Na^+, $H_2PO_4^-$, HPO_4^{2-}) were required. Reschke *et al.* (38) developed an approach to combine the dissociation equilibrium of weak electrolytes with PC-SAFT. In their work, the concentration dependence of the electrolyte dissociation was accounted for and the estimation schemes for the determination of the concentrations of the different species were formulated for mono-, di-, and triprotic acids and their salts. Therefore, in this work, the compositions of buffer components were determined by using the approach developed by Reschke *et al.* (38). The calculated compositions of buffer components are summarized in Table VI.

Dissolution Profiles and Dissolution Mechanisms of Solid Dispersions

The simultaneous dissolution profiles of indomethacin and naproxen solid dispersions in PVP K25 were measured and compared with those of the pure crystalline APIs. Moreover, the influence of API loading, type of API, temperature, stirring

Table II PC-SAFT Binary Interaction Parameters k_{ij} Used in this Work

System	$k_{ij,T}$	$k_{ij,0}$	Ref.
Indomethacin/PVP K25	−0.000633	0.0922	(34)
Naproxen/PVP K25	0.000128	−0.130	(34)
Indomethacin/Water	0.000169	−0.110	(53)
Naproxen/Water	0.000227	−0.0612	(53)
PVP K25/Water	0	−0.148	
K^+/Water	−0.00401	1.40	(58)
Na^+/Water	−0.00798	2.38	(58)
$H_2PO_4^-$/Water	0	0.25	(58)
HPO_4^{2-}/Water	0	0.25	(58)
$K^+/H_2PO_4^-$	0	0.0182	(58)
K^+/HPO_4^{2-}	0	1	(58)
$Na^+/H_2PO_4^-$	0	−0.0709	(58)
Na^+/HPO_4^{2-}	0	−1	(58)

Table III Melting Properties of Indomethacin and Naproxen Taken from (53)

API	Δh^{SL}_{0API} (kJ/mol)	T^{SL}_{0API} (K)	$\Delta c^{SL}_{p,\ 0API}$ (J/(mol K))
Indomethacin	39.2	433.2	116.9
Naproxen	31.5	429.5	87.4

speed and pH value of media on API dissolution was investigated.

The dissolution mechanisms of indomethacin and naproxen were analyzed using the chemical-potential-gradient model combined with PC-SAFT as described above. For the calculation of activity coefficients of naproxen and indomethacin in the aqueous bulk phase (γ_i^B in Eq. (5)), the presence of PVP K25 was accounted for by using PC-SAFT. In the modeling, the molar density and kinematic viscosity of water at different temperatures were calculated based on the following correlations according to the reported data in literature (59):

$$\rho/(\mathrm{mol/L}) = -0.0003\cdot(\mathrm{T}/^{\circ}\mathrm{C})^2 - 0.0008\cdot(\mathrm{T}/^{\circ}\mathrm{C}) + 55.525 \tag{41}$$

$$v/\left(\mathrm{m}^2/\mathrm{s}\right) = 2.248\cdot10^{-10}\cdot(\mathrm{T}/^{\circ}\mathrm{C})^2 - 3.195\cdot10^{-8}\cdot(\mathrm{T}/^{\circ}\mathrm{C}) + 1.572\cdot10^{-6} \tag{42}$$

The fitted parameters (k_d, k_s, K_1 and K_2) are summarized in Tables VII and VIII. Furthermore, the relation between the dissolution rates of indomethacin and PVP K25 was analyzed. Using the determined rate constants of surface reaction and diffusion (as shown in Table VII), the dissolution profiles of indomethacin in water from its solid dispersions were calculated and predicted by combining Eqs. (16), (18) and (19) with PC-SAFT.

Table IV Solubilities of Crystalline and Amorphous Naproxen as well as that of Amorphous Indomethacin in Water as Calculated from PC-SAFT

API	x^L_{API} (305.15 K) (μg/mL)	x^L_{API} (310.15 K) (μg/mL)	x^L_{API} (315.15 K) (μg/mL)
Naproxen (crystalline)	39.7780	47.5644	56.8239
Naproxen (amorphous)	532.511	556.843	584.716
Indomethacin (amorphous)	135.664	153.532	174.233

Table V Solubilities of Amorphous Indomethacin in Buffered Solutions with Different pH Values at 310.15 K as Calculated from Eq. (29)

API	x^L_{IND} (pH 4.98) (μg/mL)	x^L_{IND} (pH 6.05) (μg/mL)	x^L_{IND} (pH 7.25) (μg/mL)
Indomethacin (amorphous)	$4.70685\cdot10^2$	$4.27150\cdot10^3$	$6.59601\cdot10^4$

To evaluate the accuracy of the calculated dissolution profiles of indomethacin, the average relative deviation (ARD (%)) between the calculated and experimental data was analyzed according to Eq. (43). The calculated ARDs are presented in Table IX.

$$ARD\ (\%) = 100\ \frac{1}{n_{exp}}\sum_{m=1}^{n_{exp}}\left|\frac{x_m^{exp}-x_m^{calc}}{x_m^{exp}}\right| \tag{43}$$

Effect of API Loading on Solid Dispersion Dissolution

The simultaneous dissolution profiles of API and PVP K25 for indomethacin and naproxen solid dispersions in water at 310.15 K and at a stirring speed of 50 rpm are presented in Figs. 7 and 8. The parameters k_s, k_d, K_1 and K_2 which were fitted to the experimental dissolution profiles of indomethacin and naproxen (as shown in Figs. 7, 8, 11, 12, and 13) are listed in Tables VII and VIII, respectively.

Figure 7a shows that the dissolution of indomethacin from its solid dispersions is faster than that of its pure crystalline form, which indicates that the dissolution rate of indomethacin can be improved by preparing its amorphous solid dispersion. It also shows that the dissolution of indomethacin from solid dispersions is improved when decreasing the indomethacin loading, which is in good accordance with the observation by Mehta *et al.* (60) for API (thiazole-based leukotriene D4 antagonist) dissolution from its formulations with different loadings. Figure 7b shows that the dissolution of PVP K25 from indomethacin solid dispersions is much slower than that of pure PVP K25 and is also improved by decreasing the indomethacin loading.

Table VI Calculated Compositions of Buffer Components (K^+, Na^+, $H_2PO_4^-$, HPO_4^{2-}) in Buffer Systems with Different pH Values

	Composition (mole fraction)		
Component	pH 4.98	pH 6.05	pH 7.25
K^+	$1.20310\cdot10^{-3}$	$1.16056\cdot10^{-3}$	$6.2216\cdot10^{-4}$
Na^+	$1.420\cdot10^{-5}$	$1.6058\cdot10^{-4}$	$1.36438\cdot10^{-3}$
$H_2PO_4^-$	$1.20310\cdot10^{-3}$	$1.16056\cdot10^{-3}$	$6.2216\cdot10^{-4}$
HPO_4^{2-}	$7.10\cdot10^{-6}$	$8.029\cdot10^{-5}$	$6.8219\cdot10^{-4}$
Water	$9.9757250\cdot10^{-1}$	$9.9743801\cdot10^{-1}$	$9.9670911\cdot10^{-1}$

Table VII Parameters k_s, k_d, K_1 and K_2 Fitted to the Experimental Dissolution Profiles of Indomethacin Solid Dispersions

Conditions		k_s	k_d	K_1	K_2	k_t
50 rpm, 310.15 K, in water	$w_{IND} = 0.8$	$5.50 \cdot 10^{-7}$	$2.17 \cdot 10^{-6}$	$1.87 \cdot 10^{-5}$	$9.72 \cdot 10^{-6}$	$4.39 \cdot 10^{-7}$
	$w_{IND} = 0.4$	$7.36 \cdot 10^{-7}$	$5.36 \cdot 10^{-6}$	$9.90 \cdot 10^{-6}$	$9.53 \cdot 10^{-6}$	$6.47 \cdot 10^{-7}$
	$w_{IND} = 0.2$	$1.33 \cdot 10^{-6}$	$3.73 \cdot 10^{-5}$	$2.49 \cdot 10^{-6}$	$1.73 \cdot 10^{-5}$	$1.28 \cdot 10^{-6}$
310.15 K, $w_{IND} = 0.8$, in water	100 rpm	$6.43 \cdot 10^{-7}$	$2.50 \cdot 10^{-6}$	$1.37 \cdot 10^{-5}$	$5.42 \cdot 10^{-6}$	$5.11 \cdot 10^{-7}$
50 rpm, $w_{IND} = 0.8$, in water	305.15 K	$5.38 \cdot 10^{-7}$	$1.69 \cdot 10^{-6}$	$3.81 \cdot 10^{-5}$	$1.16 \cdot 10^{-5}$	$4.08 \cdot 10^{-7}$
50 rpm, 310.15 K, $w_{IND} = 0.8$, in buffer	pH 4.98	$9.03 \cdot 10^{-7}$	$3.08 \cdot 10^{-6}$	$3.44 \cdot 10^{-7}$	$5.56 \cdot 10^{-6}$	$6.98 \cdot 10^{-7}$
	pH 6.05	$4.56 \cdot 10^{-6}$	$1.33 \cdot 10^{-5}$	$6.43 \cdot 10^{-6}$	$1.67 \cdot 10^{-6}$	$3.39 \cdot 10^{-6}$
	pH 7.25	$5.87 \cdot 10^{-5}$	$6.38 \cdot 10^{-5}$	$2.83 \cdot 10^{-6}$	$8.14 \cdot 10^{-6}$	$3.06 \cdot 10^{-5}$

As shown in Fig. 8a, the dissolution of naproxen from its solid dispersions is also faster than that of its pure crystalline form, which implies the effectiveness of improving the dissolution rate of hydrophobic naproxen by preparing its solid dispersions using a hydrophilic polymer. Moreover, the dissolution of naproxen from solid dispersions is also improved by decreasing the naproxen loading. However, the improvement of naproxen dissolution at a loading of 0.8 compared to the dissolution of pure crystalline naproxen is much less than that at other naproxen loadings.

As found by DSC, PXRD and SEM, solid dispersions at a naproxen loading of 0.8 are crystalline, while those at naproxen loadings of 0.6, 0.4 and 0.2 are amorphous. As shown in Table V, the solubility of amorphous naproxen is more than ten times higher than that of its crystalline form and the smaller solubility of crystalline naproxen decreases the thermodynamic driving force for naproxen dissolution. This explains why the improvement of naproxen dissolution from its solid dispersion with naproxen loading of 0.8 compared to the dissolution of pure crystalline naproxen is smaller than those with lower naproxen loadings. Figure 8b shows that the dissolution of PVP K25 from naproxen solid dispersions is also much slower than that of pure PVP K25, and is also improved by decreasing the naproxen loading. Here, it needs to be mentioned that the dissolution profile of PVP K25 from solid dispersions with a naproxen loading of 0.2 could not be analyzed as described above as the absorbance of the samples was too high to be accurately detected.

Dissolution Mechanism of Solid Dispersions

As discussed in the review by Craig (18) and by Mehta *et al.* (60), the dissolution of solid dispersions can be considered as carrier-controlled for the following three cases: (1) the dissolution rates of the API from the polymer and that of polymer itself are equivalent; (2) the dissolution rates of different APIs in the same carrier are similar or identical; (3) the dissolution rate of an API from solid dispersions with different API loadings are similar or identical (*e.g.* at low API loadings≤0.2 (60)).

As shown in Figs. 7 and 8, the dissolution rates of both, indomethacin and naproxen are slower than that of PVP K25, and the dissolution rate of indomethacin from PVP K25 is slower than that of naproxen. Furthermore, the dissolution rates of both, indomethacin and naproxen increase with decreasing API loading. All these observations imply that the dissolution of indomethacin and naproxen solid dispersions with PVP K25 is not carrier-controlled, but is controlled by both, dissolution of API as well as carrier. This means that the APIs (indomethacin, naproxen) and PVP K25 co-dissolve during the solid dispersion dissolution and the dissolution of APIs (indomethacin, naproxen) and PVP K25 influence each other.

According to the simultaneous dissolution profiles of indomethacin and PVP K25 from their solid dispersions, the ratios $\theta(w_{IND})$ in Eq. (17) of the dissolution rate of indomethacin to that of PVP K25 were calculated for indomethacin loadings of 0.2, 0.4 and 0.8 according to Eq. (44) and the results are shown in Fig. 9.

$$\theta(w_{API}) = \frac{1}{n_{exp}} \sum_{i=1}^{n_{exp}} \left(\frac{\mathcal{J}_{API,i}}{\mathcal{J}_{polymer,i}} \right) \tag{44}$$

Table VIII Parameters k_s, k_d, K_1 and K_2 Fitted to the Experimental Dissolution Profiles of Naproxen Solid Dispersions

Conditions		k_s	k_d	K_1	K_2	k_t
50 rpm, 310.15 K, in water	$w_{NAP} = 0.8$	$3.76 \cdot 10^{-6}$	$3.76 \cdot 10^{-6}$	$8.32 \cdot 10^{-4}$	$5.27 \cdot 10^{-4}$	$1.88 \cdot 10^{-6}$
	$w_{NAP} = 0.6$	$2.17 \cdot 10^{-6}$	$2.96 \cdot 10^{-6}$	$5.73 \cdot 10^{-6}$	$5.73 \cdot 10^{-6}$	$1.25 \cdot 10^{-6}$
	$w_{NAP} = 0.4$	$4.41 \cdot 10^{-6}$	$1.07 \cdot 10^{-5}$	$1.58 \cdot 10^{-6}$	$1.41 \cdot 10^{-5}$	$3.12 \cdot 10^{-6}$

Table IX Average Relative Deviation (ARD) for the Calculated and Experimental Dissolution Profiles of Indomethacin Under Different Conditions

Conditions		ARD (%)
310.15 K, w_{IND} = 0.8, in water	50 rpm	11.02
	100 rpm	14.82
	150 rpm	12.83
50 rpm, w_{IND} = 0.8, in water	305.15 K	7.83
	310.15 K	11.02
	315.15 K	15.08
50 rpm, 310.15 K, w_{IND} = 0.8, in buffer	pH 4.98	17.08
	pH 6.05	23.55
	pH 7.25	18.33

As shown in Fig. 9, a linear relation between $\theta(w_{IND})$ and indomethacin loading (w_{IND}) for indomethacin solid dispersion dissolution was found in this work. This linear relation again underlines that the dissolution mechanism of indomethacin solid dispersion are both API- and carrier-controlled. It also indicates that both indomethacin and PVP K25 codissolve in proportion to their initial API loading, which belongs to one of the three mechanisms as proposed by Craig (18).

Figure 10a and b show the rate constants of surface reaction k_s and diffusion k_d for indomethacin and naproxen dissolution in water from their solid dispersions with different API loadings.

As shown in Fig. 10a, for the dissolution of indomethacin from its solid dispersions with indomethacin loadings of 0.2, 0.4 and 0.8, it is obvious that the rate constant of surface reaction k_s is smaller than that of diffusion k_d, which indicates a surface-reaction-controlled dissolution process. This means, the dissolution of indomethacin can be efficiently improved by designing its formulations or by improving its solvation performance (*e.g.* by addition of solubilizer).

As shown in Fig. 10b, the dissolution of naproxen from its solid dispersions with naproxen loading of 0.8 is controlled by both, surface reaction and diffusion, while the dissolution of naproxen at naproxen loadings of 0.4 and 0.6 is controlled by surface reaction. This observation shows that the dissolution mechanism of naproxen can be changed by changing its loading in the solid dispersions.

Figure 10 also illustrates that both, surface reaction and diffusion for amorphous indomethacin and naproxen dissolution are improved by decreasing the API loading in PVP K25. This explains the mechanism (from kinetic part) of the improvement of amorphous API dissolution by decreasing the API loading. For the dissolution of naproxen from its solid dispersions with naproxen loading of 0.8, the rate constants of both, surface reaction and diffusion are higher than those from solid dispersion with naproxen loading of 0.6. The dissolution profile (shown in Fig. 8a), however, shows a slower naproxen dissolution at a naproxen loading of 0.8. This implies that naproxen dissolution at a naproxen loading of 0.8 is also limited by its solubility (thermodynamic driving force).

From Figs. 7 and 8, it is observed that the dissolution of naproxen from its solid dispersions is faster than that of indomethacin. As listed in Table V, the solubility of amorphous naproxen is more than five times higher than that of amorphous indomethacin. Moreover, both, surface reaction rate constant and diffusion rate constant for naproxen dissolution are higher than those for indomethacin. This shows that the three main factors: higher solubility (thermodynamic driving force), higher surface reaction rate constant and higher diffusion rate constant lead to a faster dissolution of naproxen compared to indomethacin.

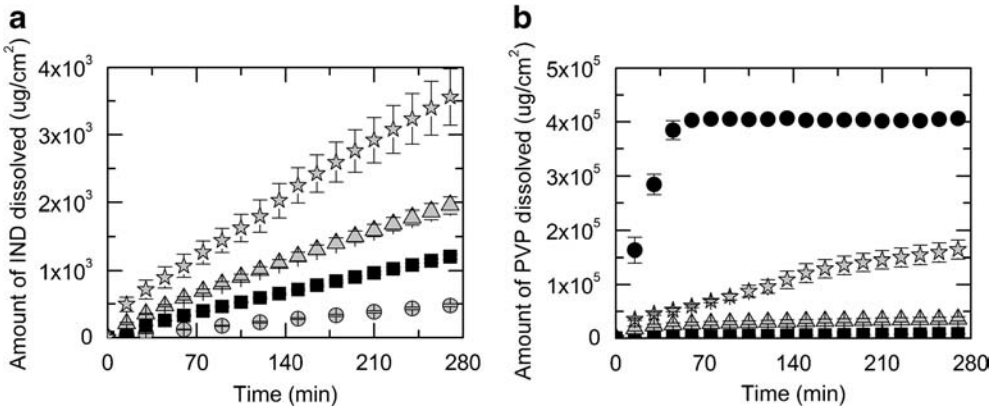

Fig. 7 Simultaneous dissolution profiles of indomethacin (**a**) and PVP K25 (**b**) from solid dispersions in water at 310.15 K and at a stirring speed of 50 rpm. In (**a**), the *gray circles*, *black squares*, *gray triangles* and *stars* represent the dissolution profiles of pure crystalline indomethacin (34) and of indomethacin from its solid dispersions with indomethacin loadings of 0.8, 0.4 and 0.2, respectively. In (**b**), the *black squares*, *gray triangles*, *stars* and *black circles* represent the dissolution profiles of PVP K25 from solid dispersions with indomethacin loadings of 0.8, 0.4, 0.2 and of pure PVP K25, respectively.

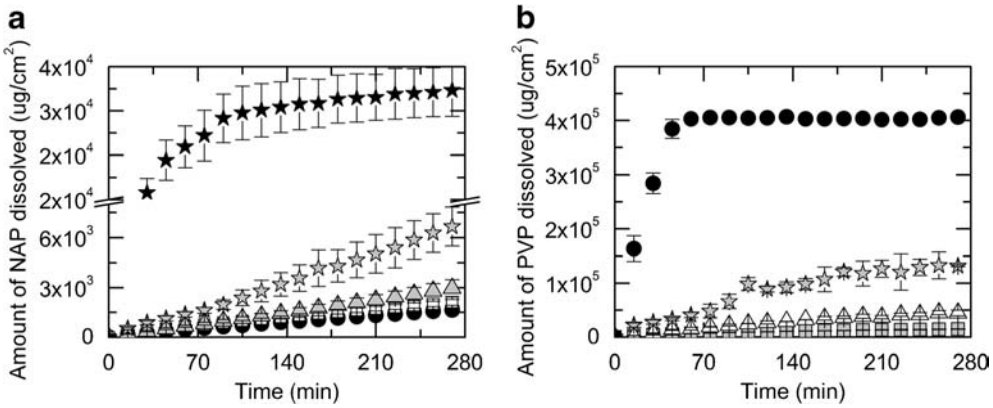

Fig. 8 Simultaneous dissolution profiles of naproxen (**a**) and PVP K25 (**b**) from solid dispersions in water at 310.15 K and at the stirring speed of 50 rpm. In (**a**), the *black circles*, *hollow squares*, *gray triangles*, *stars* and *black stars* represent the dissolution profiles of pure crystalline naproxen (34) and of naproxen from its solid dispersions with naproxen loadings of 0.8, 0.6, 0.4 and 0.2, respectively. In (**b**), the *gray squares*, *hollow triangles*, *gray stars* and *black circles* represent the dissolution profiles of PVP K25 from solid dispersions with naproxen loadings of 0.8, 0.6, 0.4 and of pure PVP K25, respectively.

Effect of Stirring Speed on Solid Dispersion Dissolution

It was known from the dissolution measurements of indomethacin solid dispersions with different indomethacin loadings (0.2, 0.4, 0.8) that the deviation of the dissolution measurements is lowest for solid dispersions with an indomethacin loading of 0.8. Therefore, in order to more accurately investigate the effect of temperature and stirring speed on indomethacin solid dispersion dissolution, the solid dispersions with an indomethacin loading of 0.8 were investigated. The dissolution profiles of indomethacin in water from its solid dispersions with indomethacin loading of 0.8 at different stirring speeds are presented in Fig. 11a. It depicts a slight improvement of indomethacin dissolution with increasing stirring speed.

The corresponding rate constants of surface reaction k_s and diffusion k_d are illustrated in Fig. 11b. It shows that the rate constant of surface reaction is smaller than that of diffusion at both stirring speeds of 50 and 100 rpm. It indicates that the dissolution process is controlled by surface reaction, which implies that the dissolution of indomethacin can be effectively improved by improving the solvation performance of indomethacin. Figure 11b also shows that the increase of stirring speed slightly improves both the surface reaction and the diffusion. The surface reaction can also be improved as the mass transport of indomethacin molecules at the solid–liquid interface is enhanced by increasing stirring speed. This implies that, with an increase of stirring speed, the dissolution rate is increased mainly due to the slight increase of surface reaction rate constant as the dissolution is identified as surface reaction controlled.

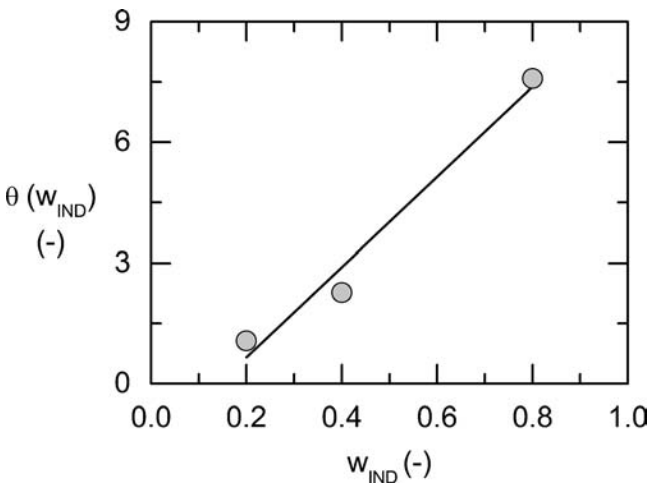

Fig. 9 The ratio (θ) of the dissolution rate of indomethacin to that of PVP K25 for its solid dispersions with indomethacin loadings of 0.2, 0.4 and 0.8. *Full line* represents a linear fitting between θ and indomethacin loading (w_{IND}) with a function of $\theta = 11.21\ w_{IND} - 1.59$.

In addition, using the determined rate constants of surface reaction and diffusion (as shown in Table VII), the dissolution profiles of indomethacin in water from its solid dispersions with indomethacin loading of 0.8 at the stirring speeds of 50 and 100 rpm were calculated and the results are also shown in Fig. 11a. As shown, the calculated results are in good accordance with the experimental data (with ARDs of 11.02% and 14.82% as shown in Table IX, respectively) although the concentrations of dissolved indomethacin are slightly overestimated. Moreover, based on a linear relation of the total rate constant of indomethacin dissolution with the stirring speed (as shown in Fig. S3 in the Supplementary Information), the dissolution profile of indomethacin from its solid dispersion at 150 rpm was predicted and is also presented in Fig. 11a. It is shown that the predicted results agree well with the experimental data with an ARD of 12.83%.

Effect of Temperature on Solid Dispersion Dissolution

The dissolution profiles of indomethacin in water from its solid dispersions with indomethacin loading of 0.8 at different temperatures are shown in Fig. 12a. It shows

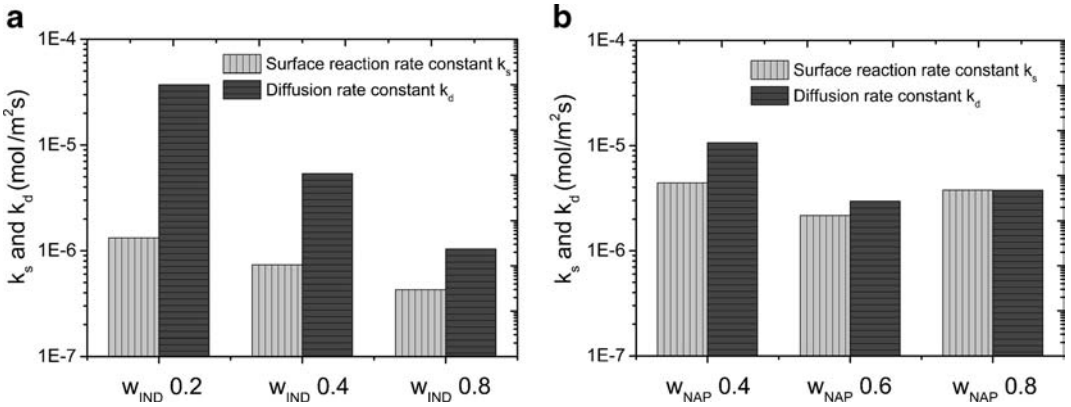

Fig. 10 Surface reaction rate constant k_s and diffusion rate constant k_d for indomethacin (**a**) and naproxen (**b**) dissolution in water from their solid dispersions with different API loadings at 310.15 K and at stirring speed of 50 rpm.

that the dissolution of indomethacin is slightly improved with increasing temperature, and the influence of temperature is smaller than that of other factors, such as indomethacin loading and stirring speed.

The corresponding rate constants of surface reaction k_s and diffusion k_d are illustrated in Fig. 12b. It shows that the rate constant of surface reaction is smaller than that of diffusion for both, 305.15 and 310.15 K. This indicates that the dissolution process at both temperatures is controlled by surface reaction. Figure 12b also shows that both, the surface reaction and diffusion, for indomethacin dissolution are slightly improved by increasing the temperature. As shown in Table V, also the solubility of amorphous indomethacin increases with increasing temperature. This implies that, with an increase of temperature, the three factors: improved solubility (thermodynamic driving force) and slightly increased k_s and k_d (from kinetic part) lead to a slight increase of the dissolution rate of indomethacin.

The dissolution profiles of indomethacin in water from its solid dispersions with indomethacin loading of 0.8 at the temperatures of 305.15 and 310.15 K were calculated and the results are also shown in Fig. 12a. As shown in Fig. 12a, the calculated results are in a good accordance with the experimental data (with ARDs of 7.83% and 11.02% as shown in Table IX, respectively), although it slightly overestimated the dissolved concentrations of indomethacin. Moreover, based on a linear relation of the total rate constant of indomethacin dissolution with the temperature (as shown in Fig. S4 in the Supplementary Information), the dissolution profile of indomethacin at 315.15 K was predicted and presented in Fig. 12a. It is shown that the predicted results are in good accordance with the experimental data with an ARD of 15.08%.

Effect of pH Value on Solid Dispersion Dissolution

The dissolution profiles of indomethacin from its solid dispersions with indomethacin loading of 0.8 in buffered solutions with pH values of 4.98, 6.05 and 7.25 at 310.15 K and at 50 rpm are shown in Fig. 13a. As to be seen, the dissolution of indomethacin at pH 4.98 is very slow, and it is improved with increasing pH of the media. The percentages of dissolved

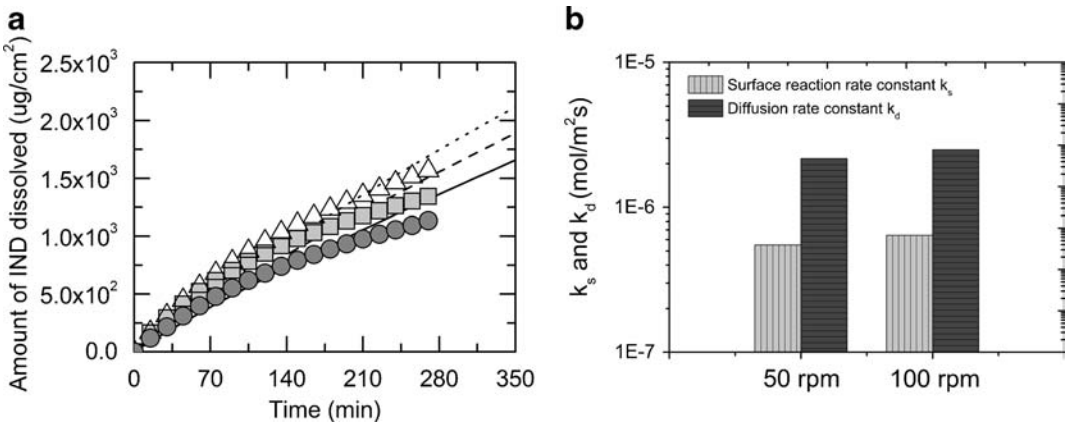

Fig. 11 (**a**) Dissolution profiles of indomethacin in water from its solid dispersions with indomethacin loading of 0.8 at 310.15 K and at stirring speeds of 50 rpm (*gray circles*), 100 rpm (*light gray squares*) and 150 rpm (*hollow triangles*). The *full (50 rpm)* and *dashed (100 rpm) lines* represent the calculated results and the *dotted (150 rpm) line* represents the predicted results using the chemical-potential-gradient model. (**b**) Surface reaction rate constant k_s and diffusion rate constant k_d for indomethacin dissolution in water from its solid dispersions with indomethacin loading of 0.8 at 310.15 K and different stirring speeds.

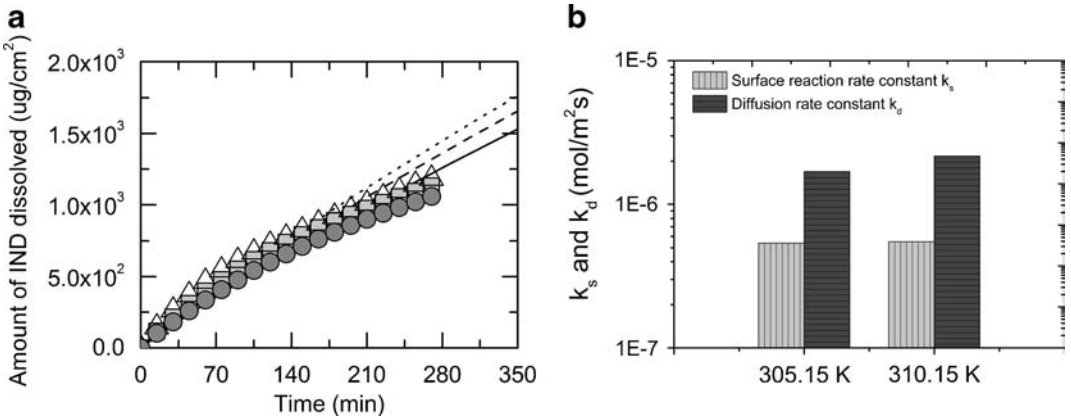

Fig. 12 (**a**) Dissolution profiles of indomethacin in water from its solid dispersions with indomethacin loading of 0.8 at 50 rpm and at the temperatures of 305.15 K (*gray circles*), 310.15 K (*light gray squares*) and 315.15 K (*hollow triangles*). The *full (305.15 K)* and *dashed (310.15 K) lines* represent the calculated results and the *dotted (315.15 K) line* represents the predicted results using the chemical-potential-gradient model. (**b**) Surface reaction rate constant k_s and diffusion rate constant k_d for indomethacin dissolution in water from its solid dispersions with indomethacin loading of 0.8 at 50 rpm and at different temperatures.

indomethacin at pH 6.05 are more than five times higher than those at pH 4.98, while the percentages of dissolved indomethacin at pH 7.25 are even more than 40 times higher than those at pH 4.98.

The respective rate constants of surface reaction k_s and diffusion k_d are illustrated in Fig. 13b. It becomes clear that the rate constant of surface reaction is smaller than that of diffusion at pH 4.98 and 6.05. This indicates that the dissolution process is controlled by surface reaction. At pH 7.25, the rate constant of surface reaction is close to that of diffusion, which indicates that the dissolution process is controlled by both surface reaction and diffusion. Figure 13b also shows that both, the surface reaction and diffusion are obviously improved by increasing pH value. As shown in Table VI, the solubility of amorphous indomethacin increases obviously with increasing pH. This implies that, with an increase of pH, the three factors of improved solubility (thermodynamic driving force), highly increased k_s and k_d (from kinetic part) lead to a considerable increase of the dissolution rate of indomethacin.

Furthermore, the dissolution profiles of indomethacin from its solid dispersions with indomethacin loading of 0.8 in buffered solutions with different pH values at 310.15 K and at 50 rpm were calculated and the results are also shown in Fig. 13a. As shown in Fig. 13a, the calculated results are in a good accordance with the experimental data.

This work shows that the developed chemical-potential-gradient model combined with PC-SAFT is suitable to calculate and even predict the dissolution profiles of indomethacin as function of stirring speed, temperature and pH value of the medium.

CONCLUSIONS

The simultaneous dissolution profiles of API and PVP K25 for indomethacin and naproxen solid dispersions

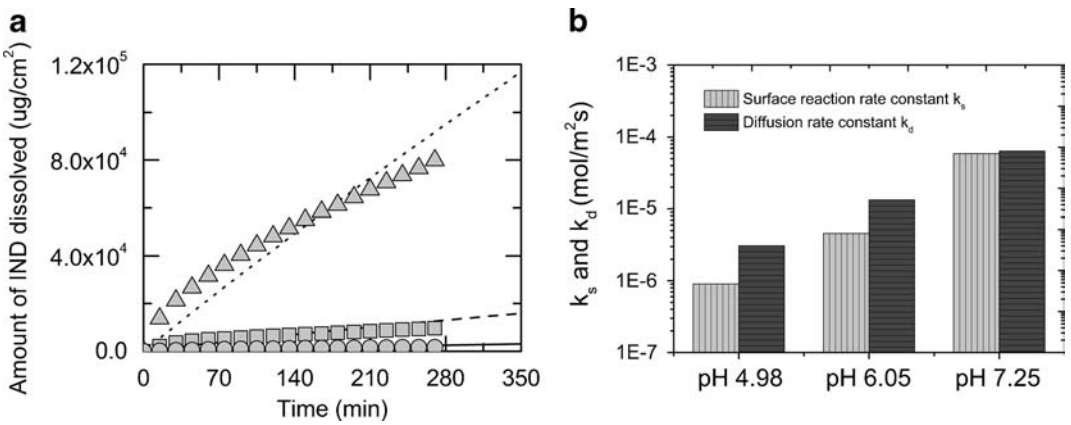

Fig. 13 (**a**) Dissolution profiles of indomethacin from its solid dispersions with indomethacin loading of 0.8 in buffered solutions with pH values of 4.98 (*gray circles*), 6.05 (*gray squares*) and 7.25 (*gray triangles*) at 310.15 K and at 50 rpm. The *full (pH 4.98)*, *dashed (pH 6.05)* and *dotted (pH 7.25) lines* represent the calculated results using the chemical-potential-gradient model. (**b**) Surface reaction rate constant k_s and diffusion rate constant k_d for indomethacin dissolution in buffered solutions with different pH from solid dispersions with indomethacin loading of 0.8 at 50 rpm and at 310.15 K.

were measured *in vitro* by using a rotating disk system. This investigation revealed that the dissolution of indomethacin and naproxen solid dispersions are both, API and carrier-controlled and both, indomethacin and naproxen, co-dissolve with PVP K25 in proportion to their initial API loading. It is also found that the dissolution rate of indomethacin and naproxen is improved by preparing its amorphous solid dispersions, by decreasing the API loading in polymer and by increasing the stirring speed, temperature and pH value of the media.

A theoretical chemical-potential-gradient model combined with PC-SAFT was developed to investigate the dissolution mechanisms of indomethacin and naproxen from their solid dispersions at different conditions. The dissolution profiles of indomethacin from their solid dispersions at different conditions could be calculated and even predicted as function of stirring speed, temperature and pH in good accordance with the experimental data. Furthermore, the modeling showed that the dissolution of indomethacin and naproxen in water from their amorphous solid dispersions is mainly controlled by surface reaction, which implies that API dissolution can be effectively improved by designing its formulation and improving the solvation performance of APIs.

More general, this work reveals that the dissolution rate J_{API} of APIs can be increased by the following factors: (1) the increased API solubility (increasing thermodynamic driving force); (2) the increased surface reaction rate constant k_s or the increased diffusion rate constant k_d or both (improving the kinetic part).

In the case that the dissolution of a solid dispersion is controlled by API dissolution or by dissolution of both, API and carrier (like in this work), the chemical-potential-gradient model can be applied to calculate and predict the dissolution profiles of the API. If dissolution of the solid dispersion is controlled by the carrier dissolution, the dissolution profile of the carrier has to be determined and the dissolution profile of the API can be predicted based on the dissolution rate of the carrier.

It also needs to be mentioned that the dissolution behaviors of solid dispersions always depend on the state of the API in polymer. Amorphous APIs are generally better soluble than their crystalline counterparts. However, they also tend to recrystallize into the low-energy crystalline form at supersaturation in the dissolution media. Although the supersaturation was not observed in this work, the dissolution behavior of solid dispersions could be affected significantly once the recrystallization occurs. Therefore, for predicting API dissolution profiles from amorphous solid dispersions, the recrystallization of amorphous APIs during solid-dispersion dissolution has to be considered when supersaturation behavior is observed.

ACKNOWLEDGMENTS AND DISCLOSURES

The authors would like to acknowledge the financial support from the Alexander von Humboldt Foundation (Yuanhui Ji) as well as that from the CLIB Graduate Cluster Industrial Biotechnology (Anke Prudic). They would like to thank Monika Meuris for assisting with the PXRD and SEM experiments. They would also like to thank the reviewers for their helpful advice.

REFERENCES

1. Newman A, Knipp G, Zografi G. Assessing the performance of amorphous solid dispersions. J Pharm Sci. 2012;101(4):1355–77.
2. Sun DD, Ju TC, Lee PI. Enhanced kinetic solubility profiles of indomethacin amorphous solid dispersions in poly(2-hydroxyethyl methacrylate) hydrogels. Eur J Pharm Biopharm. 2012;81(1):149–58.
3. Hancock BC, Parks M. What is the true solubility advantage for amorphous pharmaceuticals? Pharm Res. 2000;17(4):397–404.
4. Vasconcelos T, Sarmento B, Costa P. Solid dispersions as strategy to improve oral bioavailability of poor water soluble drugs. Drug Discov Today. 2007;12(23–24):1068–75.
5. Sivert A, Bérard V, Andrès C. New binary solid dispersion of indomethacin with surfactant polymer: from physical characterization to in vitro dissolution enhancement. J Pharm Sci. 2010;99(3):1399–413.
6. Mura P, Faucci MT, Manderioli A, Bramanti G, Parrini P. Thermal behavior and dissolution properties of naproxen from binary and ternary solid dispersions. Drug Dev Ind Pharm. 1999;25(3):257–64.
7. Kogermann K, Penkina A, Predbannikova K, Jeeger K, Veski P, Rantanen J, *et al.* Dissolution testing of amorphous solid dispersions. Int J Pharm. 2013;444(1–2):40–6.
8. Alonzo DE, Gao Y, Zhou D, Mo H, Zhang GG, Taylor LS. Dissolution and precipitation behavior of amorphous solid dispersions. J Pharm Sci. 2011;100(8):3316–31.
9. Arthur AN, Willis RW. The rate of solution of solid substances in their own solutions. J Am Chem Soc. 1897;19(12):930–4.
10. Lu AT, Frisella ME, Johnson KC. Dissolution modeling: factors affecting the dissolution rates of polydisperse powders. Pharm Res. 1993;10(9):1308–14.
11. Vudathala GK, Rogers JA. Dissolution of fludrocortisone from phospholipid coprecipitates. J Pharm Sci. 1992;81(3):282–6.
12. Higuchi T. Rate of release of medicaments from ointment bases containing drugs in suspension. J Pharm Sci. 1961;50(10):874–5.
13. Higuchi T. Mechanism of sustained-action medication. Theoretical analysis of rate of release of solid drugs dispersed in solid matrices. J Pharm Sci. 1963;52(12):1145–9.
14. Hixson AW, Crowell JH. Dependence of reaction velocity upon surface and agitation. Ind Eng Chem. 1931;23(8):923–31.
15. de Almeida LP, Simões S, Brito P, Portugal A, Figueiredo M. Modeling dissolution of sparingly soluble multisized powders. J Pharm Sci. 1997;86(6):726–32.
16. Korsmeyer RW, Gurny R, Doelker E, Buri P, Peppas NA. Mechanisms of solute release from porous hydrophilic polymers. Int J Pharm. 1983;15(1):25–35.
17. Baker RW, Lonsdale HK. Controlled release: mechanisms and rates. In: Tanquary AC, Lacey RE, editors. Controlled release of biologically active agents. Advances in experimental medicine and biology. New York: Plenum; 1974. p. 15–72.
18. Craig DQM. The mechanisms of drug release from solid dispersions in water-soluble polymers. Int J Pharm. 2002;231(2):131–44.

19. Siepmann J, Kranz H, Bodmeier R, Peppas NA. HPMC-matrices for controlled drug delivery: a new model combining diffusion, swelling, and dissolution mechanisms and predicting the release kinetics. Pharm Res. 1999;16(11):1748–56.
20. Langham ZA, Booth J, Hughes LP, Reynolds GK, Wren SA. Mechanistic insights into the dissolution of spray-dried amorphous solid dispersions. J Pharm Sci. 2012;101(8):2798–810.
21. Costa P, Sousa Lobo JM. Modeling and comparison of dissolution profiles. Eur J Pharm Sci. 2001;13(2):123–33.
22. Alonzo DE, Zhang GG, Zhou D, Gao Y, Taylor LS. Understanding the behavior of amorphous pharmaceutical systems during dissolution. Pharm Res. 2010;27(4):608–18.
23. Lu XH, Ji YH, Liu HL. Non–equilibrium thermodynamics analysis and its application in interfacial mass transfer. Sci China Chem. 2011;54(10):1659–66.
24. Liu C, Ji Y, Shao Q, Feng X, Lu X. Thermodynamic analysis for synthesis of advanced materials. In: Lu XH, Hu Y, editors. Molecular thermodynamics of complex systems, Struct Bond. Berlin: Springer–Verlag; 2009. p. 193–270.
25. Ji YH, Ji XY, Liu C, Feng X, Lu XH. Modelling of mass transfer coupling with crystallization kinetics in microscale. Chem Eng Sci. 2010;65:2649–55.
26. Ruether F, Sadowski G. Modeling the solubility of pharmaceuticals in pure solvents and solvent mixtures for drug process design. J Pharm Sci. 2009;98(11):4205–15.
27. Cassens J, Prudic A, Ruether F, Sadowski G. Solubility of pharmaceuticals and their salts as a function of pH. Ind Eng Chem Res. 2013;52(7):2721–31.
28. Fuchs D, Fischer J, Tumakaka F, Sadowski G. Solubility of amino acids: influence of the pH value and the addition of alcoholic cosolvents on aqueous solubility. Ind Eng Chem Res. 2006;45(19):6578–84.
29. Daldrup JBG, Held C, Ruether F, Schembecker G, Sadowski G. Measurement and modeling solubility of aqueous multisolute amino–acid solutions. Ind Eng Chem Res. 2010;49(3):1395–401.
30. Gross J, Sadowski G. Modeling polymer systems using the perturbed–chain statistical associating fluid theory equation of state. Ind Eng Chem Res. 2002;41(5):1084–93.
31. Tumakaka F, Gross J, Sadowski G. Modeling of polymer phase equilibria using perturbed–chain SAFT. Fluid Phase Equilib. 2002;194–197:541–51.
32. Gross J, Spuhl O, Tumakaka F, Sadowski G. Modeling copolymer systems using the perturbed–chain SAFT equation of state. Ind Eng Chem Res. 2003;42(6):1266–74.
33. Prudic A, Ji YH, Sadowski G. Thermodynamic phase behavior of API/polymer solid dispersions. Mol Pharm. 2014;11(7):2294–304.
34. Prudic A, Kleetz T, Korf M, Ji YH, Sadowski G. Influence of copolymer composition on the phase behavior of solid dispersions. Mol Pharm. 2014;11(11):4189–98.
35. Prudic A, Lesniak AK, Ji YH, Sadowski G. Thermodynamic phase behaviour of indomethacin/PLGA formulations. Eur J Pharm Biopharm. 2015; in press, doi:10.1016/j.ejpb.2015.01.029.
36. Held C, Cameretti LF, Sadowski G. Modeling aqueous electrolyte solutions: part 1. Fully dissociated electrolytes. Fluid Phase Equilib. 2008;270(1–2):87–96.
37. Held C, Sadowski G. Modeling aqueous electrolyte solutions. Part 2. Weak electrolytes. Fluid Phase Equilib. 2009;279(2):141–8.
38. Reschke T, Naeem S, Sadowski G. Osmotic coefficients of aqueous weak electrolyte solutions: influence of dissociation on data reduction and modeling. J Phys Chem B. 2012;116(25):7479–91.
39. Tumakaka F, Sadowski G. Application of the perturbed–chain SAFT equation of state to polar systems. Fluid Phase Equilib. 2004;217(2):233–9.
40. Kleiner M, Gross J. An equation of state contribution for polar components: polarizable dipoles. AIChE J. 2006;52(5):1951–61.
41. Kiesow K, Tumakaka F, Sadowski G. Experimental investigation and prediction of oiling out during crystallization process. J Cryst Growth. 2008;310(18):4163–8.
42. Gross J, Sadowski G. Perturbed–chain SAFT: an equation of state based on a perturbation theory for chain molecules. Ind Eng Chem Res. 2001;40(4):1244–60.
43. Liu R. Water-insoluble drug formulation. 2nd edition. CRC Press; 2008.
44. Dokoumetzidis A, Papadopoulou V, Valsami G, Macheras P. Development of a reaction-limited model of dissolution: application to official dissolution tests experiments. Int J Pharm. 2008;355:114–25.
45. Ward CA, Findlay RD, Rizk M. Statistical rate theory of interfacial transport. I Theoretical development. J Chem Phys. 1982;76(11):5599–605.
46. Ward CA, Rizk M, Tucker AS. Statistical rate theory of interfacial transport. II. Rate of isothermal bubble evolution in a liquid–gas solution. J Chem Phys. 1982;76(11):5606–14.
47. Dejmek M, Ward CA. A statistical rate theory study of interface concentration during crystal growth or dissolution. J Chem Phys. 1998;108(20):8698–704.
48. Prausnitz JM, Lichtenthaler RN, de Azevedo EG. Molecular thermodynamics of fluid-phase equilibria. Upper Saddle River: Prentice Hall PTR; 1999.
49. Tirkkonen S, Urtti A, Paronen P. Buffer controlled release of indomethacin from ethylcellulose microcapsules. Int J Pharm. 1995;124(2):219–29.
50. Henderson LJ. Concerning the relationship between the strength of acids and their capacity to preserve neutrality. Am J Physiol. 1908;21:173–9.
51. Henderson LJ. The theory of neutrality regulation in the animal organism. Am J Physiol. 1908;21:427–48.
52. Hansen NT, Kouskoumvekaki I, Jørgensen FS, Brunak S, Jónsdóttir SÓ. Prediction of pH-dependent aqueous solubility of druglike molecules. J Chem Inf Model. 2006;46(6):2601–9.
53. Paus R, Ji YH, Braak F, Sadowski G. Dissolution of crystalline pharmaceuticals: experimental investigation and thermodynamic modeling. Ind Eng Chem Res. 2015;54(2):731–42.
54. Gross J, Sadowski G. Application of the perturbed–chain SAFT equation of state to associating systems. Ind Eng Chem Res. 2002;41(22):5510–5.
55. Wolbach JP, Sandler SI. Using molecular orbital calculations to describe the phase behavior of cross–associating mixtures. Ind Eng Chem Res. 1998;37(8):2917–28.
56. DIN ISO 13528. Statistical methods for use in proficiency testing by interlaboratory comparisons (ISO 13528:2005). DIN Deutsches Institut für Normung e.V.; 2009. p. 98–100.
57. Legendre B, Feutelais Y. Polymorphic and thermodynamic study of indomethacin. J Therm Anal Calorim. 2004;76:255–64.
58. Held C, Reschke T, Mohammad S, Luza A, Sadowski G. ePC–SAFT revised. Chem Eng Res Des. 2014;92(12):2884–97.
59. Kestin J, Sokolov M, Wakeham WA. Viscosity of liquid water in the range −8°C to 150°C. J Phys Chem Ref Data. 1978;7(3):941–8.
60. Mehta KA, Kislalioglu MS, Phuapradit W, Malick AW, Shah NH. Effect of formulation and process variables on matrix erosion and drug release from a multiunit erosion matrix of a poorly soluble drug. Pharm Technol. 2002;2:26–34.